Remote Sensing of Environment 348 (2027) 115724

Contents lists available at ScienceDirect

Remote Sensing of Environment

journal homepage: www.elsevier.com/locate/rse

Substantial disagreement between satellite- and ground-level nighttime light patterns revealed by SDGSAT-1 and street view imagery

Yu Gong [a], Qiming Zheng [a,*], Filip Biljecki [b,c], Waishan Qiu [d], Zicheng Fan [b], Zihao Zheng [e], Lin Yan [f,g], Chun Shing Jason Pun [h], Sylvia Y. He [a]

[a] Department of Geography and Resource Management, The Chinese University of Hong Kong, Hong Kong SAR, China
[b] Department of Architecture, National University of Singapore, Singapore
[c] Department of Real Estate, National University of Singapore, Singapore
[d] Department of Urban Planning and Design, The University of Hong Kong, Hong Kong SAR, China
[e] School of Geography and Remote Sensing, Guangzhou University, Guangzhou, 510006, China
[f] School of Architecture and Urban Planning, Shenzhen University, Shenzhen, 518060, China
[g] MNR Key Laboratory for Geo-Environmental Monitoring of Great Bay Area & Guangdong Key Laboratory of Urban Informatics & Shenzhen Key Laboratory of Spatial Smart Sensing and Services, Shenzhen University, Shenzhen, 518060, China
[h] Department of Physics, The University of Hong Kong, Hong Kong SAR, China

ARTICLE INFO

Editor Name: Dr. Marie Weiss

Keywords:
Nighttime light
Remote sensing
SDGSAT-1 glimmer imagery
Nighttime street view imagery
Artificial light at night

ABSTRACT

Over the past three decades, nighttime light (NTL) has become one of the most widely used and powerful proxies for characterizing human activities. Despite the recent proliferation of available NTL data from both satellite- and ground-level sensors, intrinsic differences between these two observation approaches can result in distinct NTL brightness patterns (satellite-ground disagreement). Such disagreement, particularly its spatial heterogeneity, represents a critical yet largely overlooked issue in NTL studies, introducing uncertainty into the interpretation and application of NTL observations. Here, by incorporating SDGSAT-1 glimmer imagery and panoramic nighttime street view imagery with geospatial AI approaches, we present a spatially explicit, wall-to-wall investigation into satellite-ground disagreement across Singapore. Specifically, we characterized citywide disagreement and its variation across land-use types, analyzed contributing factors, and assessed its implications for NTL-based applications, reinforced by Monte Carlo-based uncertainty quantification and sensitivity analyses using independent observations from Singapore and Shenzhen, China. Our study revealed substantial and spatially heterogeneous satellite-ground disagreement across Singapore. Relative disagreement averaged 15% ± 13% citywide but reached 42% ± 12% in 13% of the city. Such pronounced heterogeneity was likewise evident across land-use types, with commercial areas standing out for consistently significant disagreement, where ground-level NTL brightness was 29% ± 26% higher than satellite-level NTL brightness. Building morphology, vegetation canopy cover, and sensor spectral response contributed to satellite-ground disagreement, suggestive of distinct mechanisms underlying the identified patterns. Applying satellite- and ground-level NTL data yielded relative differences of at least 115% and 83% in GDP estimation and NTL exposure inequality assessment, respectively. This study sheds new light on satellite-ground disagreement by moving beyond discrete comparisons toward a comprehensive analysis of its heterogeneity and implications, thereby establishing an empirical basis for integrating NTL observations and contributing to more reliable NTL-based applications and evidence-informed policies on sustainable urbanization.

1. Introduction

The stark contrast between brightly lit urban hubs and dark undeveloped regions in nighttime light (NTL) data offers compelling and intuitive evidence of human presence (Levin et al., 2020; Li et al., 2026; Shi et al., 2023). Over the past three decades, satellite-level NTL imagery has become an indispensable source for mapping socioeconomic distributions (Amaral et al., 2005; Tan et al., 2018), evaluating regional

* Corresponding author.
E-mail address: qmzheng@cuhk.edu.hk (Q. Zheng).

https://doi.org/10.1016/j.rse.2026.115724
Received 1 June 2026; Received in revised form 2 October 2026; Accepted 6 October 2026
Available online 13 October 2026
0034-4257/© 2026 The Authors. Published by Elsevier Inc. This is an open access article under the CC BY-NC license (http://creativecommons.org/licenses/by-nc/4.0/).

electrification (He et al., 2023; Shi et al., 2016), tracking urban expansion (Chen et al., 2026; Gao et al., 2016), and monitoring light pollution (Falchi et al., 2016; Weber et al., 2025). Despite advantages in broad spatial coverage, high overpass frequency, and streamlined data processing, satellite-level NTL observations primarily record upward light emissions due to the top-down viewing geometry (Kocifaj et al., 2023; Levin, 2023). However, NTL exposure experienced by humans and natural ecosystems is not determined solely by upward-directed emissions. A widespread mesh of artificial light sources, such as vehicle headlights, billboards, building façades, and indoor light leakage, emits a substantial fraction of light horizontally (Fig. 1a) (Ho and Lin, 2015; Li et al., 2020b; Ngarambe and Kim, 2018). As a result, the restricted viewing geometry of satellite sensors hampers their ability to capture the full complexity of light emissions, risking underrepresentation of the brightening nighttime environment and biased assessments of NTL exposure for urban populations and natural ecological systems.

Beyond satellite-level observations, growing efforts have turned to ground-level sensing approaches to characterize NTL patterns. With finer spatial granularity, multidirectional sensing capability, and greater sensitivity to artificial light within complex urban structures, ground-level NTL observations can better represent local lighting conditions and lived experiences from a human-scale perspective (Fig. 1a) (Levin, 2023; Muñoz-Gil et al., 2022). Nevertheless, most ground-level NTL observations, including those measured using Sky Quality Meters (SQMs) (Kyba et al., 2012), multispectral photometers (Aubé et al., 2020), and spectrometers (Kocifaj et al., 2023), are subject to labor-intensive collection and limited representativeness, as they are typically acquired at spatially discrete locations. Recent advances in nighttime street view imagery (SVI) and geospatial AI have enabled a novel ground-level approach to monitor citywide and spatially continuous NTL patterns (Dai et al., 2026; Fan and Biljecki, 2024; Wang et al., 2026b; Ye et al., 2025). By capturing surrounding lighting conditions from a human-scale vantage point, nighttime SVI, particularly panoramic imagery with a 360° field of view, offers several merits, making it a promising complement to satellite-level NTL imagery: (1) rich information on both the intensity and semantic context of lighting sources; (2) detailed characterization of vertically distributed lighting (e.g., building façade lighting); (3) low-cost data acquisition using consumer-grade cameras and publicly accessible platforms (e.g., Mapillary); and (4) enhanced representation of NTL patterns through overlapping observations from adjacent locations (Kang et al., 2020).

The proliferation of both satellite- and ground-level NTL observations, together with their complementary advantages, has spurred the integrated use of multi-level NTL data. However, intrinsic differences in sensing approaches render satellite- and ground-level observations as distinct representations of the nighttime environment, giving rise to disagreement between satellite- and ground-level NTL brightness patterns (hereafter referred to as "satellite-ground disagreement").

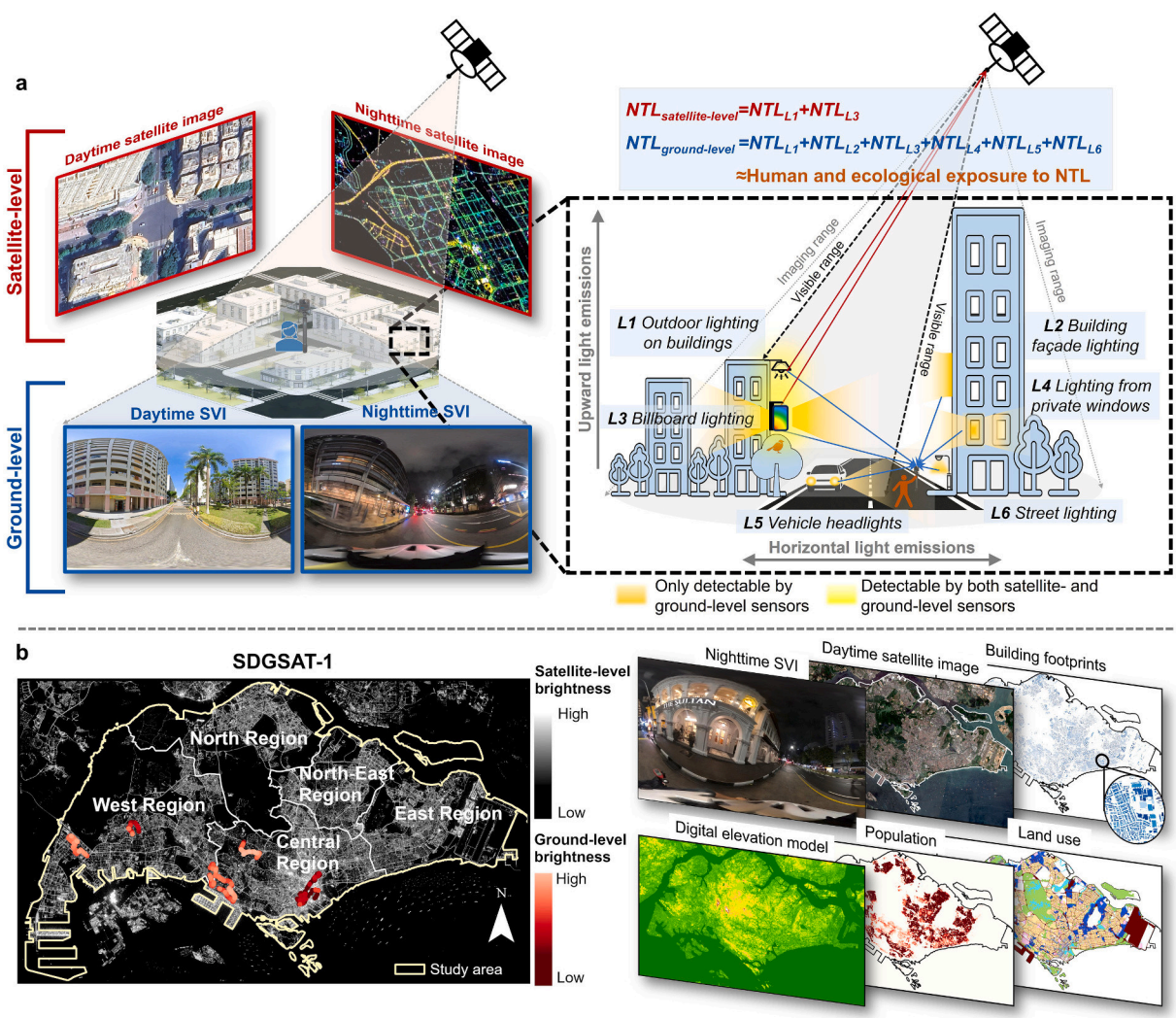

Fig. 1. Conceptual diagram: (a) comparison between satellite- and ground-level NTL observations; (b) study area and datasets. (For interpretation of the references to colour in this figure legend, the reader is referred to the web version of this article.)

Although such disagreement is theoretically expected and has been reported in recent studies based on spatially discrete ground-level measurements (e.g., using SQMs and multispectral photometers), its spatial heterogeneity within cities and across different urban forms and environmental contexts has been scarcely explored and remains a critical yet largely overlooked issue in NTL studies (Katz and Levin, 2016; Labrousse et al., 2025; Levin, 2023). This oversight hinders our understanding of the spatial comparability of different NTL observations. More importantly, it may mask pronounced local disagreement behind citywide averages, propagate substantial uncertainty into NTL-based applications, and impede the effective integration of satellite- and ground-level NTL observations.

Against this backdrop, our study incorporates high-resolution SDGSAT-1 glimmer imagery and panoramic nighttime SVI with geospatial AI approaches to provide citywide, spatially explicit insights into satellite-ground disagreement. Taking Singapore as a case study, we focus on the spatial heterogeneity of such disagreement. Specifically, we address three critical questions:

- **How do they disagree:** How do NTL brightness patterns derived from satellite-level observations (SDGSAT-1 glimmer imagery) differ from those derived from ground-level observations (nighttime SVI), and how does the resulting satellite-ground disagreement vary within a highly urbanized environment?
- **Why do they disagree:** What are the contributing factors to the satellite-ground disagreement?
- **What are the implications of the disagreement:** How does the satellite-ground disagreement influence NTL-based applications?

In an era of increasingly available multi-level NTL observations, our comprehensive and in-depth insights into satellite-ground disagreement represent an important prerequisite for interpreting and integrating NTL observations in remote sensing. Such understanding paves the way for more robust NTL-based applications and supports initiatives and policies related to sustainable urbanization, such as the United Nations Sustainable Development Goals (SDGs) Target 7.3 on energy efficiency and Target 11.6 on reducing environmental impact of cities.

2. Study area and datasets

2.1. Study area

We examined satellite-ground disagreement in Singapore, a highly urbanized metropolis characterized by diverse land-use types and substantial spatial variations in population density and nighttime lighting conditions. Specifically, Singapore comprises five Level-1 (L1) regions: the Central Region is the most densely developed area, dominated by residential and commercial areas; the North Region includes extensive green space and dense vegetation; the West Region contains a large proportion of industrial areas; and the East Region and the North-East Region are mainly residential areas (Fig. 1b). Singapore also exhibits pronounced vertical heterogeneity, with building heights ranging from 4 to 70 stories, resulting in widespread yet varying degrees of building obstruction across the city that may further affect NTL observations (Yeh and Yuen, 2010). These diverse urban contexts, coupled with the availability of high-quality and comparable nighttime SVI, render Singapore an ideal study area for investigating citywide satellite-ground disagreement. Furthermore, we selected Shenzhen, China, as an independent cross-city validation area to assess the generalizability and robustness of the disagreement patterns observed in Singapore.

2.2. Datasets and preprocessing

2.2.1. SDGSAT-1 glimmer imagery

Launched in 2021, SDGSAT-1 is equipped with a glimmer imager that provides multispectral imagery in red, green, and blue (RGB) bands at a spatial resolution of 40 m, as well as panchromatic imagery in panchromatic low (PL) and panchromatic high (PH) bands at a spatial resolution of 10 m (Guo et al., 2023a; Huang et al., 2025; Wang et al., 2025). Three cloud-free SDGSAT-1 glimmer images were acquired for Singapore (29 June 2023 at 22:41 and 01 August 2025 at 22:05 local time) and Shenzhen (26 November 2025 at 21:08 local time), which had undergone radiometric calibration, band registration, and orthorectification (CBAS, 2022; Yan et al., 2024). We further performed targeted preprocessing to enhance data quality, including denoising (Wang et al., 2024), georeferencing, and radiance correction (Gong et al., 2025; Wu et al., 2024). Given the identical spectral responses, PL and PH bands were averaged to represent satellite-level NTL brightness (CBAS, 2022; Jiang et al., 2024).

2.2.2. Nighttime street view imagery

We obtained 2831 panoramic nighttime SVIs across Singapore to characterize ground-level lighting conditions (hereafter referred to as the NightSVI-SG_{Fan} dataset; Fig. 1b). As the primary dataset for quantifying satellite-ground disagreement, NightSVI-SG_{Fan} was collected from August to November 2023 between 20:00 and 23:00 local time and exhibited representative coverage of Singapore's diverse urban environments, including high- and low-rise residential and commercial areas, industrial zones, highway regions, communities, and university campuses (Fan and Biljecki, 2024).

Additionally, two field surveys were conducted to collect independent panoramic nighttime SVIs between 20:00 and 23:00 local time using a GoPro Max2 360 camera mounted at a fixed height of 1.7 m under consistent camera settings, including ISO, exposure, shutter speed, and white balance. Specifically, 3011 images acquired in Singapore in July 2026 (hereafter referred to as the NightSVI-SG_{Yu} dataset) were used for cross-dataset validation and uncertainty quantification, while 390 images acquired in Shenzhen from December 2025 to January 2026 constituted the NightSVI-SZ dataset and were used for cross-city validation. We avoided data collection during holidays, such as Christmas Day and New Year's Day, to improve the representativeness of the imagery and reduce potential biases in NTL observations caused by ephemeral activities.

2.2.3. Other datasets

The following auxiliary datasets were also employed in this study (see Table S1 for further details): (1) daytime SVI retrieved through the Google Street View (GSV) API using 10-m grid coordinates derived from SDGSAT-1 panchromatic glimmer imagery. After quality control, i.e., the exclusion of blurred and indoor panoramas, 552,451 GSV images were retained and semantically segmented (Supplementary Text 1; Fig. S1); (2) multispectral NTL imagery acquired from the International Space Station (ISS) over Singapore on 27 June 2025 at 00:13 (local time) using a Nikon Z 9 digital camera; (3) cloud-free Sentinel-2 surface reflectance imagery covering Singapore on 24 July 2023 accessed via the Google Earth Engine platform; (4) building footprints from the GLObal Building heights for Urban Studies dataset (Kamath et al., 2024); (5) digital elevation model data at a resolution of 30 m; (6) road networks from OpenStreetMap; (7) GDP statistics from the Singapore Department of Statistics; (8) administrative boundaries and land-use data from the Urban Redevelopment Authority of Singapore Master Plan 2019; and (9) population data for Singapore in 2023 from the WorldPop Global Demographic Data Project at a resolution of approximately 100 m at the equator (see Table S1).

3. Methods

The methodological framework consists of four parts (Fig. 2): (1) mapping spatially continuous, wall-to-wall ground-level NTL brightness across Singapore; (2) characterizing satellite-ground disagreement; (3) analyzing contributing factors associated with the disagreement; and (4) assessing implications of the disagreement for two representative NTL-

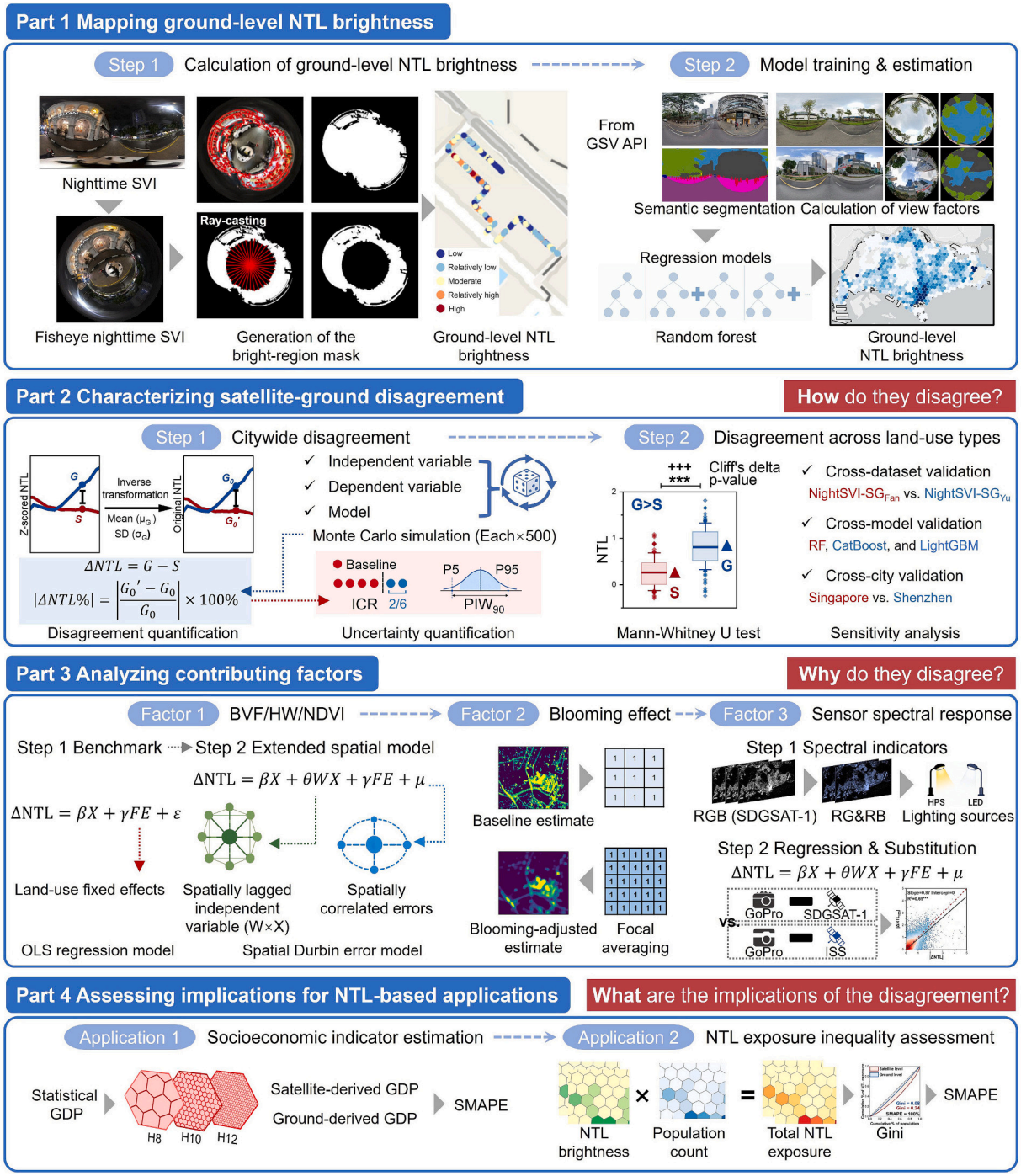

Fig. 2. Methodological framework of this study. (For interpretation of the references to colour in this figure legend, the reader is referred to the web version of this article.)

based applications, namely socioeconomic indicator estimation and NTL exposure inequality assessment. Two points warrant clarification. First, although artificial light at night (ALAN) and NTL differ slightly, the two terms are often used interchangeably. For consistency, we use NTL throughout this study. Second, this study focuses on differences between satellite- and ground-level NTL brightness, without treating either as the ground truth or a benchmark.

3.1. Mapping wall-to-wall ground-level NTL brightness

3.1.1. Measuring ground-level NTL brightness from nighttime SVI

We extended the method established by Fan and Biljecki (2024) to derive ground-level NTL brightness from nighttime SVI. The procedure began by converting panoramic SVI into a fisheye projection to account for geometric distortions in equirectangular imagery, particularly around high-rise buildings, and to better represent the surrounding lighting environment (Fig. 3a). The resulting RGB fisheye imagery was then transformed into corresponding brightness imagery (Eq. 1; Fig. 3b). To isolate bright areas while suppressing fragmented noise, we delineated continuous contours in each brightness image and filled the areas enclosed by these contours, yielding a binary bright-region mask (Fig. 3c–d). This contour-based mask cannot, however, distinguish genuinely bright regions from unlit areas enclosed within the detected contours, making central ground areas prone to misclassification as

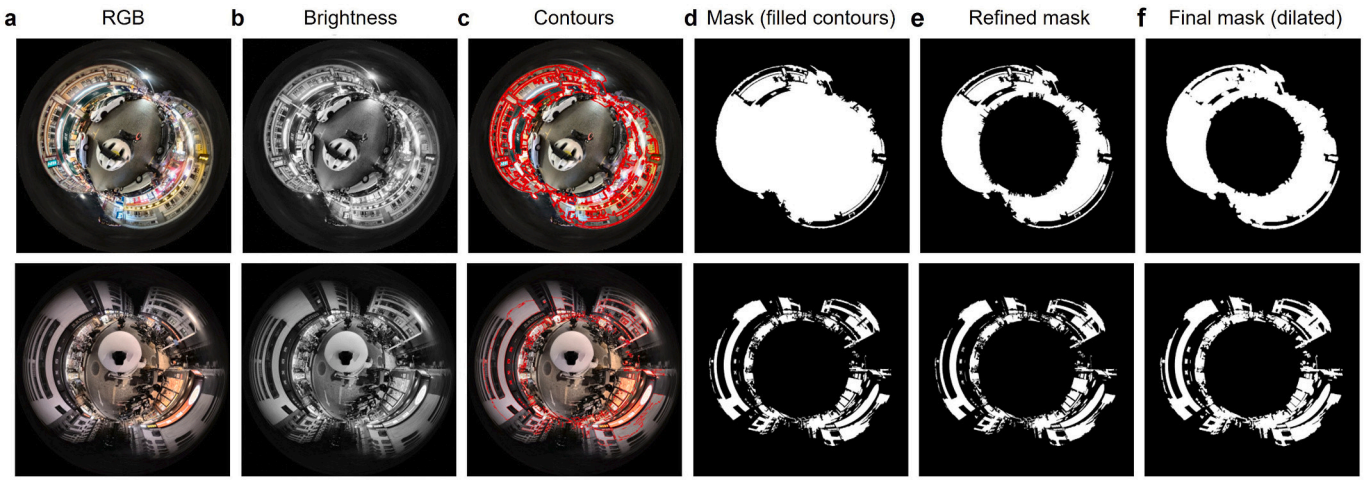

Fig. 3. Workflow for generating the binary bright-region mask. (For interpretation of the references to colour in this figure legend, the reader is referred to the web version of this article.)

bright areas and introducing biases arising from variations in surface colour and material (Fig. 3d). To address this issue, we developed a ray-casting method by emitting rays from the image center toward surrounding bright areas along uniformly spaced radial directions (Fig. 2). For each ray, the area between the image center and the first detected bright boundary was masked out (Fig. 3e). Morphological dilation was subsequently applied to smooth the mask boundaries and ensure complete coverage of bright areas (Fig. 3f). Finally, brightness values within the refined binary bright-region mask were summed to derive total brightness. Considering the viewing geometry of panoramic nighttime SVI, which captures the visible lighting environment from multiple directions, this total brightness metric was interpreted as an integrated measure of human-scale NTL conditions visible from the imaging location (Fig. S2) (Biljecki and Ito, 2021; Fan and Biljecki, 2024).

$$Brightness = 0.299 \times R + 0.587 \times G + 0.114 \times B \quad (1)$$

where *Brightness* denotes the NTL brightness; *R*, *G*, and *B* denote values for the red, green, and blue bands, respectively.

3.1.2. Estimating wall-to-wall ground-level NTL brightness across Singapore

Machine learning was utilized to estimate ground-level NTL brightness across Singapore based on the NightSVI-SG_{Fan} dataset, with 10-m SDGSAT-1 grids serving as the basic spatial units for matching different geospatial datasets. First, brightness derived from nighttime SVI was spatially assigned to the corresponding grid according to its imaging locations. For grids intersecting multiple nighttime SVIs, the associated brightness values were averaged to represent ground-level NTL brightness. Based on the literature, we constructed a comprehensive set of independent variables from three aspects: satellite-level NTL intensity, surface radiation and environment, and building morphology (see Table S2 for details) (Kocifaj, 2018; Li et al., 2025; Luginbuhl et al., 2009; Pan and Du, 2021; Wallner and Kocifaj, 2019). After quality control, 1796 training samples and 427,741 prediction samples were retained. The training samples encompassed diverse urban contexts of Singapore, covering various land-use types, building environments, NTL brightness levels, and population densities (Fig. S3). They also showed broad coverage of the prediction domain, with 99.7% ± 0.5% (mean ± SD; SD denotes standard deviation) of prediction samples falling within the ranges of the training samples, supporting the feasibility of wall-to-wall ground-level NTL brightness estimation (Table S3).

Seven regression models were evaluated: linear regression (LR), Light Gradient Boosting Machine (LightGBM), random forest (RF), categorical boosting (CatBoost), eXtreme Gradient Boosting (XGBoost), K-nearest neighbors (KNN) regression, and multi-layer perceptron (MLP). We assessed model performance using 10-fold cross-validation, with the coefficient of determination (R^2) and mean absolute percentage error (MAPE) adopted as accuracy metrics. The model achieving the highest R^2 and lowest MAPE was applied to generate wall-to-wall estimates of ground-level NTL brightness. To further assess the reliability of the resulting estimates, we conducted a cross-dataset validation by comparing them against independent observations from the NightSVI-SG_{Yu} dataset across 877 spatially matched grids. Given differences in camera systems, acquisition conditions, and observation periods, this validation was designed to assess the consistency of spatial brightness patterns rather than absolute agreement in brightness.

3.2. Characterizing satellite-ground disagreement

3.2.1. Quantifying citywide satellite-ground disagreement

We aggregated satellite- and ground-level NTL brightness into a common H3 framework by averaging values within hexagons at three analytical resolutions: level 8 (H8; edge length: ~531 m), level 10 (H10; 76 m), and level 12 (H12; 11 m). This aggregation was motivated by two considerations. First, hexagons are less susceptible to biases arising from edge effects than square grids (Bousquin, 2021). Second, the spatial resolutions of hexagons broadly align with the most widely used satellite-level NTL imagery, including VIIRS (500 m), Luojia-1 (130 m), and SDGSAT-1 (10 m). Notably, satellite-level NTL brightness at all three analytical resolutions was derived from the same SDGSAT-1 imagery, thereby minimizing confounding effects introduced by differences among sensors, including, but not limited to, overpass time (Guo et al., 2023b; Levin, 2025) and low-light detection sensitivity (CBAS, 2022; Guo et al., 2023a).

We developed two complementary metrics to quantify satellite-ground disagreement: absolute disagreement (ΔNTL) and relative disagreement (|ΔNTL%|) (Fig. 2). Satellite- and ground-level NTL brightness were first logarithmically transformed to reduce the influence of extreme values and distributional skewness, and then z-score standardized to enable direct comparison between the two observation approaches (Helbich et al., 2021). While radiometric calibration allows for physical interpretation of NTL brightness, it comes with downsides, particularly the need for specialized calibration procedures and reference measurements (de Miguel et al., 2021; Yin et al., 2020). *Z*-score standardization is technically simple and flexible, offering broader practical applicability and transferability while preserving relative spatial patterns. Unless specified, all NTL brightness values are presented on a z-scored basis. ΔNTL, defined as the difference between z-scored ground- and satellite-level NTL brightness (Eq. 2), provided an

intuitive representation of the disagreement pattern, i.e., whether ground-level NTL brightness was higher than satellite-level NTL brightness (hereafter denoted as G>S) or lower (G<S). However, because ΔNTL is dimensionless, its magnitude lacks direct physical interpretability. We therefore derived |ΔNTL%| by adopting an inverse transformation approach which mapped both observations onto a common ground-level brightness scale: (1) back-transforming the z-scored ground-level NTL brightness to its original scale (G_0; Eq. 3); (2) applying the ground-level standardization parameters (μ_G and σ_G) to the z-scored satellite-level NTL brightness (G_0'; Eq. 4); and (3) calculating |ΔNTL%| as the absolute percentage difference between G_0' and G_0 (Eq. 5). As a relative metric, |ΔNTL%| was sensitive to low ground-level NTL brightness in dark areas and was therefore interpreted alongside ΔNTL to comprehensively quantify satellite-ground disagreement.

$$\Delta NTL = G - S \tag{2}$$

$$G_0 = e^{\sigma_G \times G + \mu_G} \tag{3}$$

$$G_0{}' = e^{\sigma_G \times S + \mu_G} \tag{4}$$

$$|\Delta NTL\%| = |\frac{G_0{}' - G_0}{G_0}| \times 100\% \tag{5}$$

where S and G denote the z-scored satellite- and ground-level NTL brightness after logarithmic transformation; G_0 represents the original ground-level NTL brightness; μ_G and σ_G are the mean and standard deviation parameters used for z-score standardization of ground-level NTL brightness; G_0' denotes the transformed satellite-level NTL brightness.

Additionally, we developed a Monte Carlo framework to quantify how uncertainties associated with ground-level NTL brightness estimation propagate into satellite-ground disagreement. Three major sources of uncertainty were considered: independent variable uncertainty, dependent variable uncertainty, and model uncertainty, with their respective quantification procedures detailed in Supplementary Text 2. For each uncertainty source, 500 Monte Carlo simulations were performed, during which ground-level NTL brightness was re-estimated under perturbed conditions and the resulting satellite-ground disagreement (i.e., ΔNTL and |ΔNTL%|) was recalculated. The propagated uncertainty was evaluated using two complementary metrics: the inconsistency ratio (ICR; Eq. 6), defined as the proportion of simulations in which the pattern of ΔNTL (i.e., G>S or G<S) differed from the baseline disagreement pattern; and the 90% prediction interval width (PIW_{90}; Eq. 7), characterizing the uncertainty range of |ΔNTL%| (Liu et al., 2023; Meinshausen and Ridgeway, 2006; Wei et al., 2025).

$$ICR = \frac{M}{N_{MC}} \times 100\% \tag{6}$$

$$PIW_{90} = P_{95} - P_5 \tag{7}$$

where M denotes the number of simulations in which the pattern of ΔNTL differs from the baseline estimate; N_{MC} denotes the total number of Monte Carlo simulations (N_{MC}=500 in this study); P_5 and P_{95} denote the 5th and 95th percentiles of the simulated |ΔNTL%| values, respectively.

3.2.2. Characterizing satellite-ground disagreement across land-use types

Given the association between land-use types and NTL brightness, we further examined satellite-ground disagreement across land-use types to provide a more semantically explicit characterization of its spatial heterogeneity (Table S4). This analysis was performed at the H12 resolution, as coarser H8 and H10 hexagons are more likely to contain mixed land-use compositions. Specifically, within each land-use type, we compared the distributions of satellite- and ground-level NTL brightness using the Mann-Whitney U test to evaluate whether they differed significantly (Fig. 2). However, the large sample sizes at the H12 resolution may inflate the sensitivity of the Mann-Whitney U test, making p-values less informative for detecting practical significance (Lin et al., 2013). Consequently, we paired the p-value with Cliff's delta (δ) as a complementary effect-size metric to distinguish substantive disagreement from statistical artifacts (Cliff, 1993). Cliff's delta ranges from −1 to 1, with $|\delta|<0.147$ indicating a negligible effect, $0.147\leq|\delta|<0.33$ a small effect, $0.33\leq|\delta|<0.474$ a medium effect, and $|\delta|\geq0.474$ a large effect (Romano et al., 2006). Since all $|\delta|$ values remained below 1 in this study, the identified disagreement pattern, i.e., G>S or G<S, should be interpreted as an overall tendency within each land-use type, while localized regions with the opposite disagreement pattern may still exist.

To assess the robustness and generalizability of the identified satellite-ground disagreement across land-use types, we performed three sensitivity analyses. **(1) Cross-dataset validation.** We applied the same analytical framework to two independent nighttime SVI datasets in Singapore, i.e., NightSVI-SG_{Fan} and NightSVI-SG_{Yu}, to examine whether disagreement patterns were consistent across different ground-level NTL observations. **(2) Cross-model validation.** We compared satellite-ground disagreement derived from different ground-level NTL brightness estimation models to evaluate the stability of disagreement patterns across modeling approaches. **(3) Cross-city validation.** Satellite-ground disagreement across land-use types was further characterized in Shenzhen using the NightSVI-SZ dataset to examine whether the disagreement patterns observed in Singapore persisted beyond a single urban context.

3.3. Analyzing contributing factors to satellite-ground disagreement

We examined five potential contributing factors spanning three thematic aspects, informed by previous studies and feature importance derived from the RF model (see Supplementary Text 3 for details). **(1) Building morphology.** Given the key role of the blocking effect in regulating upward light emissions, it can be assumed that ground-level sensors would capture stronger NTL signals than satellite sensors in dense urban canyons (Kocifaj, 2018; Li et al., 2022; Wu et al., 2025). We therefore considered two potential contributing factors: building view factor (BVF), defined as the proportion of the overlying hemisphere obstructed by building structures and derived from semantically segmented GSV imagery, and height-to-width ratio (HW), which characterizes street-canyon geometry through the relationship between building height and street width (Table S2). **(2) Vegetation canopy cover.** Acknowledging that vegetation can obstruct NTL emissions and modify the bidirectional reflectance distribution function of surfaces, we incorporated the normalized difference vegetation index (NDVI) as a potential contributing factor to the disagreement (Li et al., 2025; Tan et al., 2022; Wang et al., 2021). **(3) Sensor-related effect.** Considering the characteristics of both the SDGSAT-1 glimmer sensor and the GoPro camera, especially the near-nadir viewing geometry of SDGSAT-1, we posit that the blooming effect and sensor spectral response mismatch may contribute to the satellite-ground disagreement (Shi et al., 2025; Zheng et al., 2020). In contrast, the angular effect is expected to play a limited role, especially relative to wide-swath satellite sensors such as VIIRS (Supplementary Text 3; Fig. S4).

Based on the properties of the five potential contributing factors, we adopted two approaches to quantify their associations with satellite-ground disagreement, represented by ΔNTL. For BVF, HW, and NDVI, we implemented a multivariable regression approach. Potential multicollinearity was assessed using variance inflation factors, with all values below 3, indicating no substantial multicollinearity (Table S5). The benchmark ordinary least squares (OLS) regression model included land-use fixed effects to account for systematic differences in satellite-ground disagreement across land-use types (Eq. 8). To address spatial dependence, we further extended this benchmark model to a spatial Durbin error model (SDEM) by incorporating spatially lagged independent variables and spatially correlated error terms (Eqs. 9 and 10) (Fang et al., 2022; Yang et al., 2022).

$$\Delta\text{NTL} = \beta X + \gamma FE + \varepsilon \quad (8)$$

$$\Delta\text{NTL} = \beta X + \theta WX + \gamma FE + \mu \quad (9)$$

$$\mu = \lambda W\mu + \varepsilon \quad (10)$$

$$X = (BVF, HW, NDVI, RG, RB) \quad (11)$$

where β and θ are vectors of coefficients associated with the independent variables and their spatial lags, respectively; X denotes the vector of independent variables; FE represents land-use fixed effects; γ denotes the coefficients of land-use fixed effects; W represents the spatial weights matrix constructed based on K-nearest neighbors; μ is the spatially correlated error term; λ is the spatial error coefficient; ε is the independent error term; RG represents the red-to-green ratio derived from SDGSAT-1 multispectral glimmer imagery; RB represents the red-to-blue ratio.

As for the blooming effect, we applied focal averaging to the baseline estimates of ground-level NTL brightness using two moving windows: 3 × 3 (30 m × 30 m) and 5 × 5 (50 m × 50 m). This allowed us to simulate the blooming of brightness inherent in satellite-level NTL imagery (Fig. 2). By comparing the resulting blooming-adjusted estimates with the baseline estimates, we assessed the contribution of the blooming effect to the identified satellite-ground disagreement.

For sensor spectral response, we adopted a two-pronged approach to measure its contribution to satellite-ground disagreement. The panchromatic SDGSAT-1 glimmer sensor covers a spectral response range of 444–910 nm, whereas the GoPro camera records signals primarily within the visible spectrum of 400–700 nm. Contemporary outdoor lighting is dominated by two major technologies: high pressure sodium (HPS) lamps, characterized by golden-orange light with an emission peak at 819 nm in the near-infrared (NIR) band, and light emitting diodes (LED) lamps, which emit across 400–800 nm with a blue-band peak at 450–460 nm (Fig. 4) (Elvidge et al., 2010). Therefore, SDGSAT-1 is more sensitive to NIR emissions of HPS lamps, while GoPro cameras effectively capture blue-band emissions of LED lamps. Based on this theoretical evidence, we hypothesize that variations in spectral response contribute to the satellite-ground disagreement, where ground-level sensors are expected to record lower NTL brightness than satellite-level sensors in HPS-dominated areas (G<S), but higher brightness in LED-dominated areas (G>S).

To examine this hypothesis, we first derived two spectral indicators from SDGSAT-1 multispectral glimmer imagery: the red-to-green ratio (RG) and the red-to-blue ratio (RB). Lower values indicate a higher proportion of LED lamps and higher values are associated with HPS-dominated areas (Jia et al., 2024). Both indicators were incorporated into the regression models (Eqs. 8 and 9). Under our hypothesis, lower RG and RB should be associated with positive ΔNTL (G>S) and higher values should correspond to negative ΔNTL (G<S), together yielding negative correlations with ΔNTL. Second, we conducted a substitution analysis by replacing SDGSAT-1 imagery with ISS NTL imagery (Fig. 2). Given the same spectral response range of the GoPro camera and the ISS sensor (the Nikon camera) across the 400–700 nm spectrum, ISS-derived NTL brightness patterns are expected to be more comparable with GoPro-derived NTL patterns. Accordingly, if sensor spectral response contributes to the identified disagreement, this substitution should reduce the magnitude of ΔNTL, i.e., $|\Delta\text{NTL}_{\text{ISS}}| < |\Delta\text{NTL}|$.

$$\Delta NTL_{ISS} = G - ISS \quad (12)$$

where ΔNTL_{ISS} is the absolute disagreement between ground-level NTL brightness and ISS-derived NTL brightness; G is the z-scored ground-level NTL brightness; ISS denotes the z-scored NTL brightness derived from ISS NTL imagery.

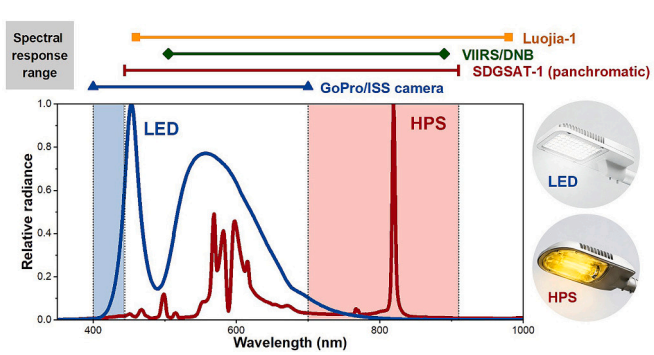

Fig. 4. Emission spectra of a 1000 W HPS lamp and an LED lamp, together with the spectral response ranges of the sensors mentioned in this study. (For interpretation of the references to colour in this figure legend, the reader is referred to the web version of this article.)

3.4. Assessing implications of satellite-ground disagreement for NTL-based applications

To quantify the implications of satellite-ground disagreement for downstream NTL-based analyses, we conducted two representative applications using established methods and compared the outcomes derived from satellite- and ground-level NTL observations (Fig. 2). It should be noted that neither satellite- nor ground-derived outcomes were considered as a reference. Instead, this analysis was to quantify the extent to which the resulting outcomes differed when different NTL observations were adopted. **(1) Estimating gross domestic product (GDP).** Based on official GDP statistics, we adopted a spatial disaggregation approach to estimate hexagon-level GDP using both satellite- and ground-level NTL brightness (see Supplementary Text 4 for details). **(2) Assessing NTL exposure and its inequality.** Total NTL exposure was estimated by multiplying NTL brightness by population counts, and its inequality was subsequently quantified using the Gini coefficient (Chen et al., 2022). For both applications, we used the original satellite- and ground-level NTL brightness and employed the symmetric mean absolute percentage error (SMAPE) to quantify the relative differences between satellite- and ground-derived outcomes (Eq. 13). SMAPE ranges from 0 to 200%, and higher SMAPE values correspond to larger differences.

$$SMAPE_{GDP} = \frac{|GDP_{satellite} - GDP_{ground}|}{(GDP_{satellite} + GDP_{ground})/2} \times 100\% \quad (13)$$

where $SMAPE_{GDP}$ is the relative difference; $GDP_{satellite}$ is the satellite-derived GDP estimate; GDP_{ground} is the ground-derived GDP estimate. This equation can be extended to quantify the relative difference in NTL exposure inequality by replacing GDP with the corresponding Gini coefficient.

4. Results

4.1. Estimation of wall-to-wall ground-level NTL brightness

Across the seven models evaluated for estimating ground-level NTL brightness across Singapore, the RF model achieved the best 10-fold cross-validation performance ($R^2 = 0.73$; MAPE = 33%; Fig. 5a), with estimated ground-level NTL brightness closely aligned with observed values along the 1:1 reference line (Fig. 5b). CatBoost and LightGBM demonstrated comparable but slightly lower accuracy (Fig. 5a). Consequently, RF-estimated ground-level NTL brightness was used in subsequent analyses. Independent cross-dataset validation further revealed an acceptable and statistically significant correlation between RF estimates derived from the NightSVI-SG_{Fan} dataset and observed ground-level NTL brightness from the NightSVI-SG_{Yu} dataset (Pearson correlation coefficient $r = 0.69$; $p < 0.001$; Fig. 5c), albeit with differences in camera

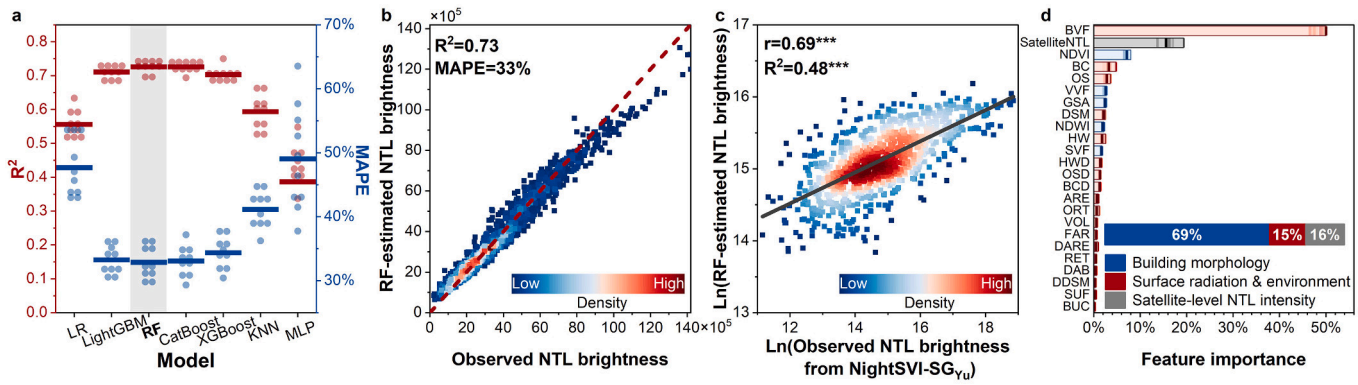

Fig. 5. Model performance: (a) accuracy metrics, where solid circles denote individual results and horizontal lines indicate mean values; (b) RF-estimated versus observed ground-level NTL brightness using the NightSVI-SG_{Fan} dataset; (c) RF-estimated ground-level NTL brightness based on the NightSVI-SG_{Fan} dataset versus independent observations from the NightSVI-SG_{Yu} dataset; (d) feature importance of the RF model. *: $p < 0.05$; **: $p < 0.01$; ***: $p < 0.001$. (For interpretation of the references to colour in this figure legend, the reader is referred to the web version of this article.)

systems, acquisition conditions, and observation periods between the two datasets. This cross-dataset consistency corroborates the reliability of the wall-to-wall ground-level NTL brightness estimates. Feature importance analysis highlighted the dominant role of building morphology features in the RF model, which accounted for 69% of the total importance, with BVF alone contributing 50% (Fig. 5d). In comparison, surface radiation and environment features contributed 15% in total, while satellite-level NTL intensity contributed 16%, indicating relatively modest contributions to ground-level NTL brightness estimation.

4.2. Citywide satellite-ground disagreement

We observed substantial and spatially heterogeneous disagreement between satellite- and ground-level NTL brightness across Singapore (Fig. 6). At the H8 resolution, ΔNTL revealed a nearly balanced bidirectional pattern: 48% of areas exhibited higher ground-level NTL brightness (G>S; ΔNTL = 0.48 ± 0.52, mean ± SD), whereas the remaining 52% exhibited higher satellite-level NTL brightness (G<S; ΔNTL = −0.44 ± 0.35; Fig. 6f). Despite this nearly balanced split, pronounced absolute disagreement was evident across 35% of the city: 16% exhibited a marked G>S pattern (ΔNTL > 0.5) and 19% showed a marked G<S pattern (ΔNTL < −0.5; Fig. 6c). A similar bidirectional disagreement pattern was empirically observed across analytical resolutions (Figs. S5-S6). At the H10 resolution, 48% and 52% of areas showed G>S (ΔNTL = 0.58 ± 0.53) and G<S (ΔNTL = -0.53 ± 0.45), respectively, whereas at H12, the corresponding proportions shifted to 45% and 55%, with mean ΔNTL values of 0.72 ± 0.63 and − 0.58 ± 0.46, respectively. Relative disagreement likewise exhibited substantial spatial heterogeneity. At the H8 resolution, |ΔNTL%| averaged 15% ± 13% across the city, while 39% of areas showed above-average disagreement (23% ± 13%) and 13% reached more than twice the citywide average (42% ± 12%; Fig. 6d). In addition, |ΔNTL%| increased toward finer analytical resolutions. Specifically, |ΔNTL%| increased to 21% ± 20% at H10 and 27% ± 24% at H12, representing increases of 40% and 80% relative to the H8 value, respectively.

We further quantified the propagation of uncertainties associated with ground-level NTL brightness estimation into ΔNTL and |ΔNTL%| (Fig. 7). Overall, the Monte Carlo analysis demonstrated that the identified citywide satellite-ground disagreement remained robust to the three uncertainty sources. For independent variable uncertainty, the average ICR across the city was 3%, with 90% of areas showing ICR below 5%, indicating highly consistent satellite-ground disagreement patterns (i.e., G>S or G<S) across most areas (Fig. 7a). The average PIW_{90} also revealed a narrow uncertainty range (5%), suggesting only trivial perturbations in the magnitude of |ΔNTL%| (Fig. 7b). Model uncertainty had a similarly limited influence, with average ICR and PIW_{90} of 5% and 11%, respectively (Fig. 7e–f). In comparison, dependent variable uncertainty produced relatively higher uncertainty, with average ICR and PIW_{90} of 18% and 22%, which was likely related to variability embedded in the paired ground-level NTL observations acquired under different conditions (Supplementary Text 2). Nevertheless, ICR and PIW_{90} remained below 25% in 75% and 73% of areas, respectively, supporting the robustness of the identified disagreement patterns across most of Singapore (Fig. 7c).

4.3. Heterogeneous satellite-ground disagreement across land-use types

Satellite-ground disagreement showed pronounced spatial heterogeneity across land-use types (Fig. 8). A predominant fraction of commercial areas (|ΔNTL%| = 29% ± 26%), institutional areas (24% ± 25%), green space (30% ± 27%), and residential areas (23% ± 18%) exhibited higher ground-level NTL brightness than satellite-level NTL brightness (G>S). Among these four land-use types, commercial and residential areas stood out with statistically significant disagreement with non-negligible effect sizes ($p < 0.001$; $|\delta| \geq 0.147$; Fig. 8b–c). In contrast, despite moderate |ΔNTL%| with statistical significance in institutional areas and green space, negligible effect sizes indicated by Cliff's delta suggested limited practical differences between satellite- and ground-level NTL brightness. Industrial and transport areas followed the opposite G<S pattern with lower ground-level NTL brightness. Transport areas showed particularly pronounced disagreement, with an average |ΔNTL%| of 31% ± 30% and a medium effect size ($p < 0.001$; $|\delta| \geq 0.33$).

Sensitivity analyses further demonstrated the robustness and generalizability of the satellite-ground disagreement patterns, including cross-dataset validation using observed ground-level NTL brightness from different nighttime SVI datasets (Fig. 9), cross-model validation using estimated ground-level brightness from different models (Fig. 10), and cross-city validation in Shenzhen (Fig. 11). Overall, the identified disagreement across land-use types showed high consensus across all sensitivity analyses. In particular, commercial areas stood out with the most robust pattern, consistently showing significant G>S disagreement with non-negligible effect sizes. Residential and transport areas likewise retained their respective G>S and G<S patterns across analyses, although their statistical significance varied. These variations were observed in validations using spatially discrete ground-level NTL observations, potentially reflecting limited sampling representativeness within individual land-use types (Fig. 9). This suggests that sparse observations may introduce sampling-related uncertainty into the characterization of land-use-dependent disagreement, whereas wall-to-wall estimation enables a more comprehensive representation of its spatial

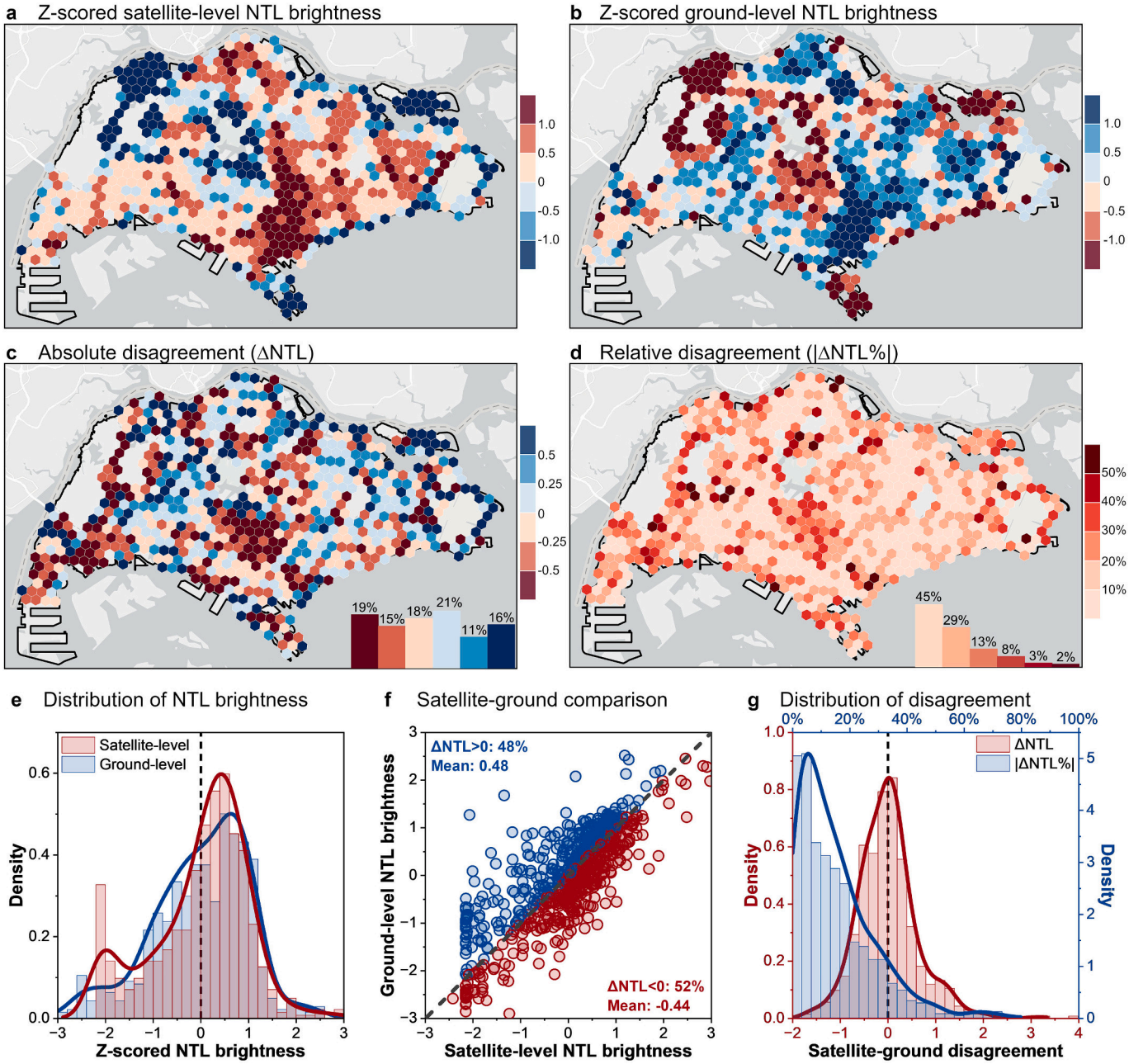

Fig. 6. Satellite-ground disagreement at the H8 resolution: (a) z-scored satellite-level NTL brightness; (b) z-scored ground-level NTL brightness; (c) absolute disagreement; (d) relative disagreement; (e) distributions of independently z-scored satellite- and ground-level NTL brightness; (f) z-scored ground-level versus satellite-level NTL brightness; (g) distributions of ΔNTL and |ΔNTL%|. (For interpretation of the references to colour in this figure legend, the reader is referred to the web version of this article.)

heterogeneity.

4.4. From observation to explanation: Contributing factors to satellite-ground disagreement

Regression analyses revealed distinct associations between ΔNTL and the potential contributing factors. BVF was consistently and positively associated with ΔNTL across different model specifications and analytical resolutions, e.g., OLS regression models with and without land-use fixed effects (Table 1). While for HW, its association with ΔNTL became weaker and generally insignificant after including BVF in the regression models, indicating a limited contribution beyond that of BVF. For NDVI, although the magnitude and significance of its association with ΔNTL varied across model specifications and analytical resolutions, all statistically significant coefficients were positive. Notably, these findings remained robust after spatial autocorrelation was accounted for using SDEM under alternative spatial weights matrices, with both BVF and NDVI showing significant positive associations with ΔNTL (β_{BVF}=0.771–0.807; β_{NDVI}=0.472–0.543; $p < 0.001$; Table S6). Meanwhile, the SDEM effectively eliminated residual spatial autocorrelation: Moran's I decreased from 0.41 ($p < 0.001$) to near-zero and statistically insignificant values ($p > 0.5$; Table S6).

These results suggest that both building morphology and vegetation canopy cover contribute to the identified satellite-ground disagreement. Specifically, highly enclosed built environments, where buildings occupy a larger proportion of the visible hemisphere, are more likely to exhibit higher ground-level than satellite-level NTL brightness, reflecting greater obstruction of upward light emissions from reaching satellite

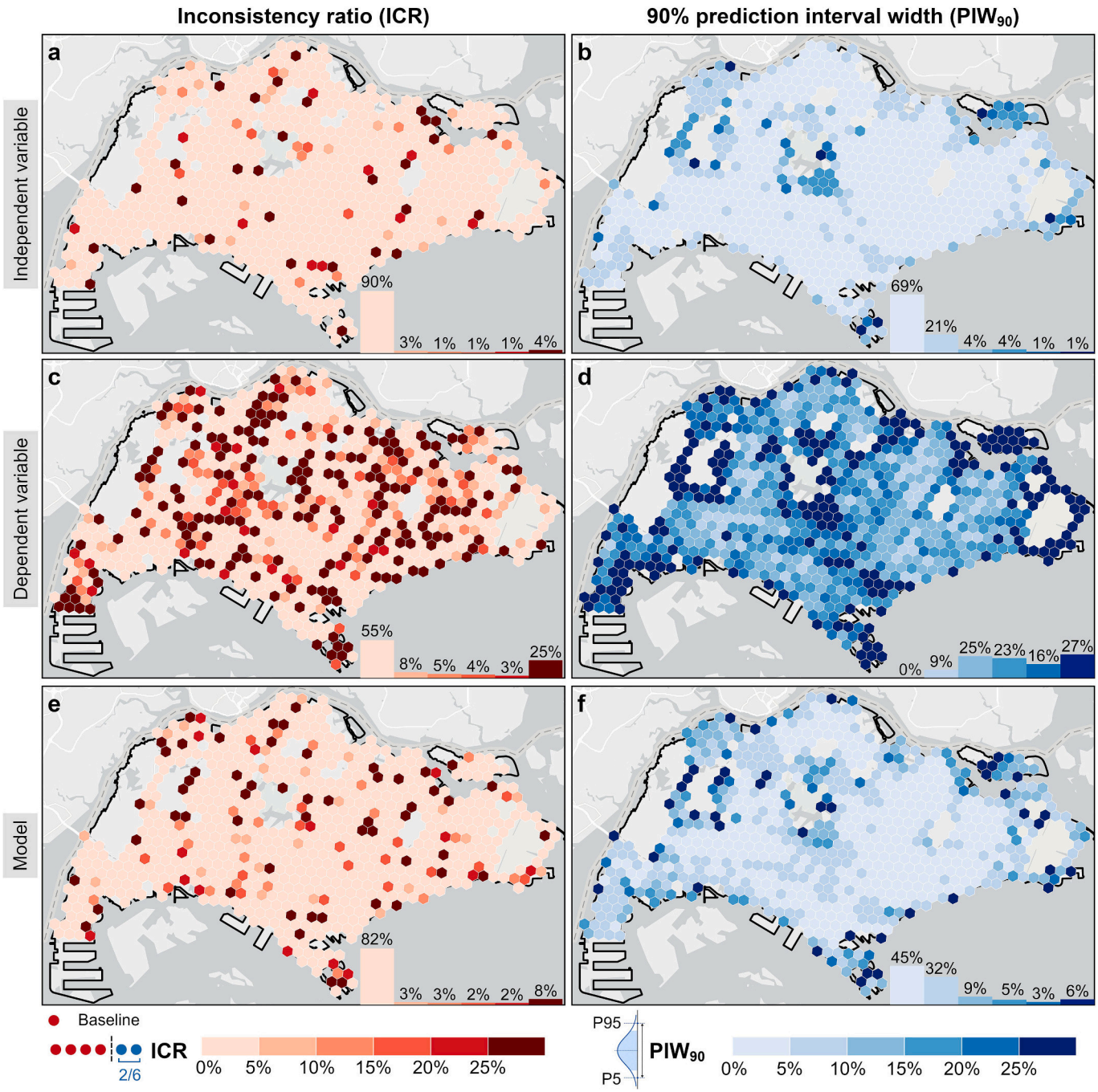

Fig. 7. Propagated uncertainty in satellite-ground disagreement: (a–b) independent variable uncertainty; (c–d) dependent variable uncertainty; (e–f) model uncertainty. (For interpretation of the references to colour in this figure legend, the reader is referred to the web version of this article.)

sensors. Although HW also showed a generally positive association with ΔNTL, its weaker and less stable contribution suggests that visible built surfaces represented by BVF were more closely related to satellite-ground disagreement than street-canyon geometry alone. Dense vegetation cover was likewise associated with higher ΔNTL, potentially due to vegetation-induced obstruction and attenuation of upward light emissions.

As for the blooming effect, we observed that blooming-adjusted estimates of both ΔNTL and |ΔNTL%| closely matched the baseline estimates across the city, with values concentrated around the 1:1 line regardless of the size of the moving window applied (Fig. 12a–b). Moreover, blooming adjustment resulted in negligible changes in satellite-ground disagreement patterns across land-use types. For example, commercial areas showed only minor deviations between the baseline and the two blooming-adjusted estimates, with maximum changes of only 0.04 in ΔNTL and 2% in |ΔNTL%| (Fig. 12c). These results indicate a marginal influence of the blooming effect on the identified satellite-ground disagreement.

Finally, our analysis showed that sensor spectral response contributed to the satellite-ground disagreement (Fig. 13). First, compared with spectral indicator RB, RG showed a more consistent and statistically significant negative association with ΔNTL (Table 1), supporting our hypothesis that LED-dominated areas with lower RG values exhibited a G>S pattern, whereas HPS-dominated areas with higher RG values tended toward G<S disagreement. Second, replacing SDGSAT-1 NTL brightness with ISS-derived NTL brightness further corroborated the

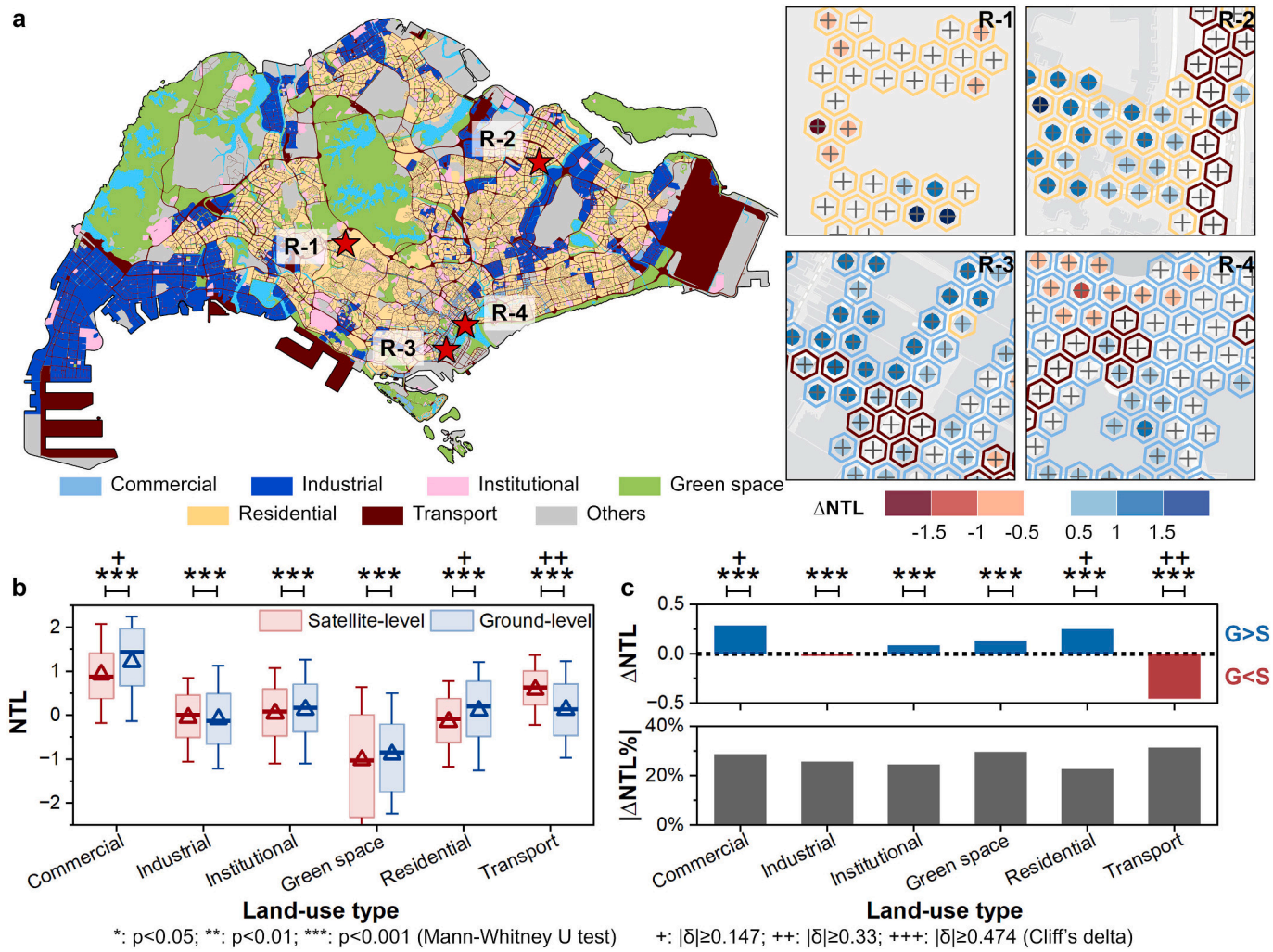

Fig. 8. Satellite-ground disagreement across land-use types: (a) spatial distributions, with hexagon outlines indicating land-use types and circles representing absolute disagreement (ΔNTL); (b) z-scored satellite- and ground-level NTL brightness; (c) ΔNTL and relative disagreement (|ΔNTL%|). Gray plus signs in (a) indicate significant disagreement with non-negligible effect sizes ($p < 0.001$; $|\delta| \geq 0.147$). (For interpretation of the references to colour in this figure legend, the reader is referred to the web version of this article.)

contribution of sensor spectral response to the satellite-ground disagreement. Specifically, we observed consistently lower $|\Delta NTL_{ISS}|$ than $|\Delta NTL|$ across the three analytical resolutions, evidenced by regression slopes below 1 (Fig. 13a–c). This provides evidence that sensor pairs sharing comparable spectral responses exhibit lower absolute disagreement relative to sensor pairs with different spectral responses. Overall, differences in sensor spectral response constitute a crucial contributing factor to the satellite-ground disagreement.

4.5. From observation to application: Impacts of satellite-ground disagreement

Fig. 14 presents the resulting GDP estimates using different NTL observations, revealing marked differences between satellite- and ground-derived outcomes. SMAPE values further showed that these differences were both pronounced and spatially heterogeneous. For instance, at the H8 resolution, the average SMAPE was approximately 115%, with a considerable proportion of areas (61%) exhibiting extremely large differences between satellite- and ground-derived GDP estimates (SMAPE > 100%). The differences became more pronounced toward finer analytical resolutions, with the average SMAPE increasing to 130% at H10 and 138% at H12.

When assessing NTL exposure, satellite- and ground-derived estimates also revealed different patterns of exposure inequality (Fig. 15). At the H8 resolution, the Gini coefficient was substantially lower for ground-derived NTL exposure (0.08) than for satellite-derived NTL exposure (0.24), corresponding to a considerable difference in NTL exposure inequality (SMAPE = 100%). This pattern persisted at the H10 (SMAPE = 87%) and H12 (SMAPE = 83%) resolutions, consistently indicating a more even distribution of ground-derived NTL exposure and greater inequality in satellite-derived NTL exposure across Singapore. Moreover, the absolute difference in Gini coefficients also increased progressively toward finer analytical resolutions, rising from 0.16 at H8 to 0.20 at H10 and 0.24 at H12.

5. Discussion

5.1. Heterogeneous satellite-ground disagreement

Our comprehensive, fine-grained assessment reveals substantial, spatially heterogeneous, and bidirectional satellite-ground disagreement, encompassing both G>S and G<S patterns. Monte Carlo analysis further supported the robustness of these disagreement patterns to uncertainties associated with ground-level NTL brightness estimation. Satellite-ground disagreement also varied systematically across land-use types, showing broadly consistent patterns across datasets, modeling

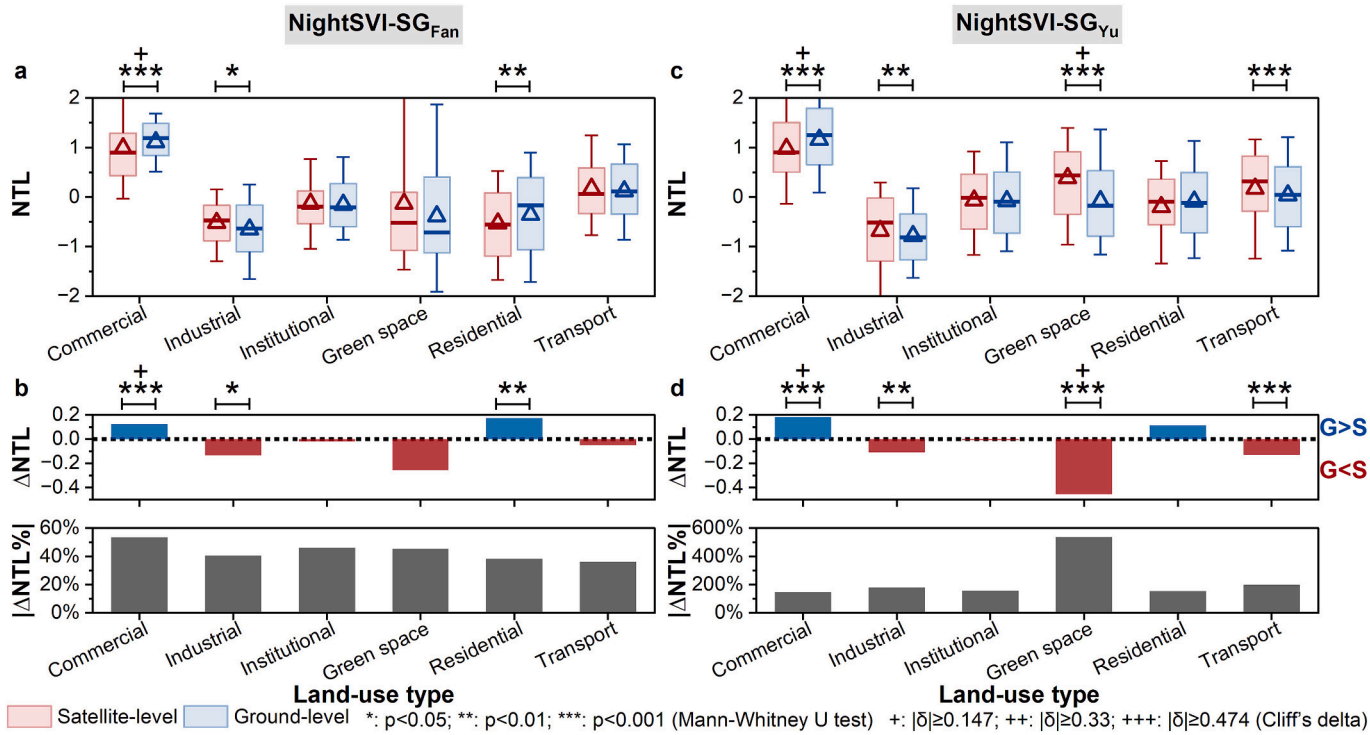

Fig. 9. Cross-dataset validation of satellite-ground disagreement across land-use types: (a–b) NightSVI-SG$_{Fan}$ dataset; (c–d) NightSVI-SG$_{Yu}$ dataset. (For interpretation of the references to colour in this figure legend, the reader is referred to the web version of this article.)

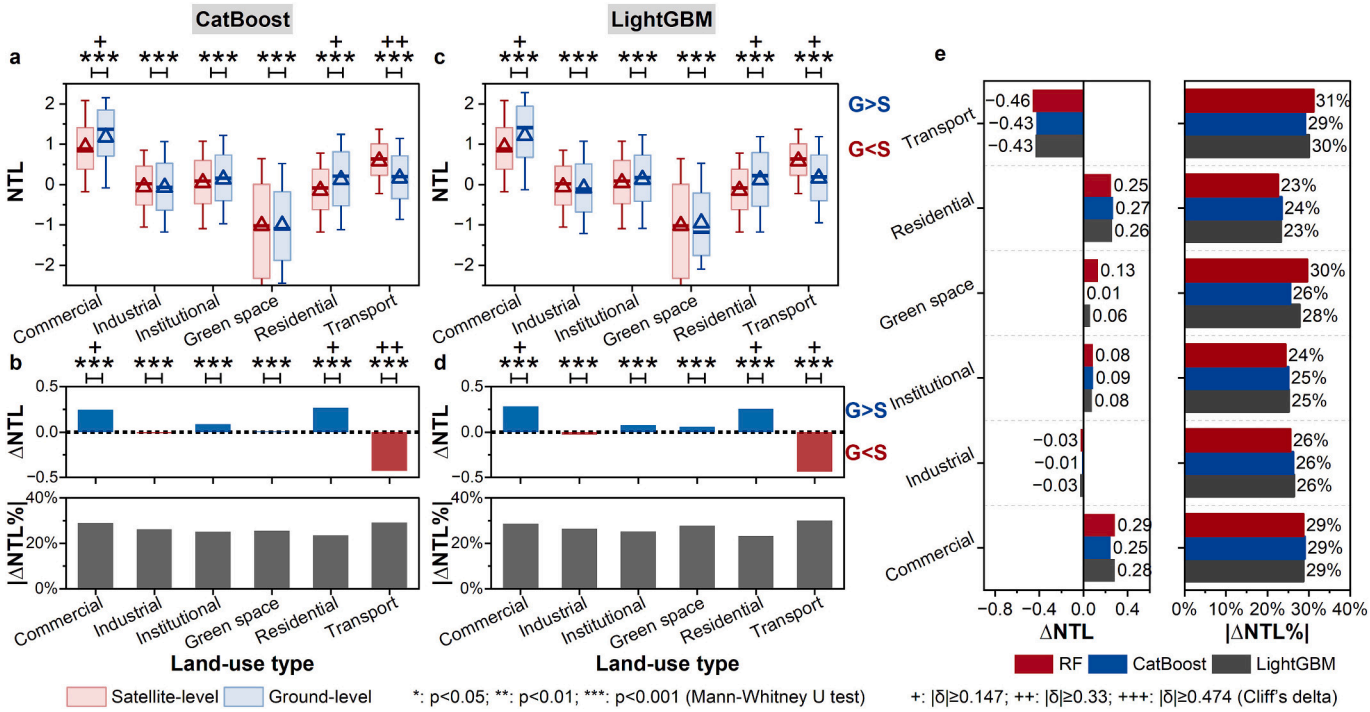

Fig. 10. Cross-model validation of satellite-ground disagreement across land-use types: (a–b) CatBoost; (c–d) LightGBM; (e) absolute disagreement (ΔNTL) and relative disagreement (|ΔNTL%|) derived from RF, CatBoost, and LightGBM. (For interpretation of the references to colour in this figure legend, the reader is referred to the web version of this article.)

approaches, and cities. Commercial and residential areas generally exhibited higher ground-level NTL brightness (G>S). In commercial areas, concentrated artificial light from shops and billboards can amplify the relative contribution of laterally emitted light to ground-level NTL observations, while surrounding buildings can obstruct part of these emissions from reaching satellite sensors, plausibly explaining the observed G>S pattern (Levin, 2023). For residential areas, the G>S disagreement may be related to the presence of lighting sources that are prominent at the human scale but less visible from above, such as brightly illuminated hawker centers beneath covered canopies and

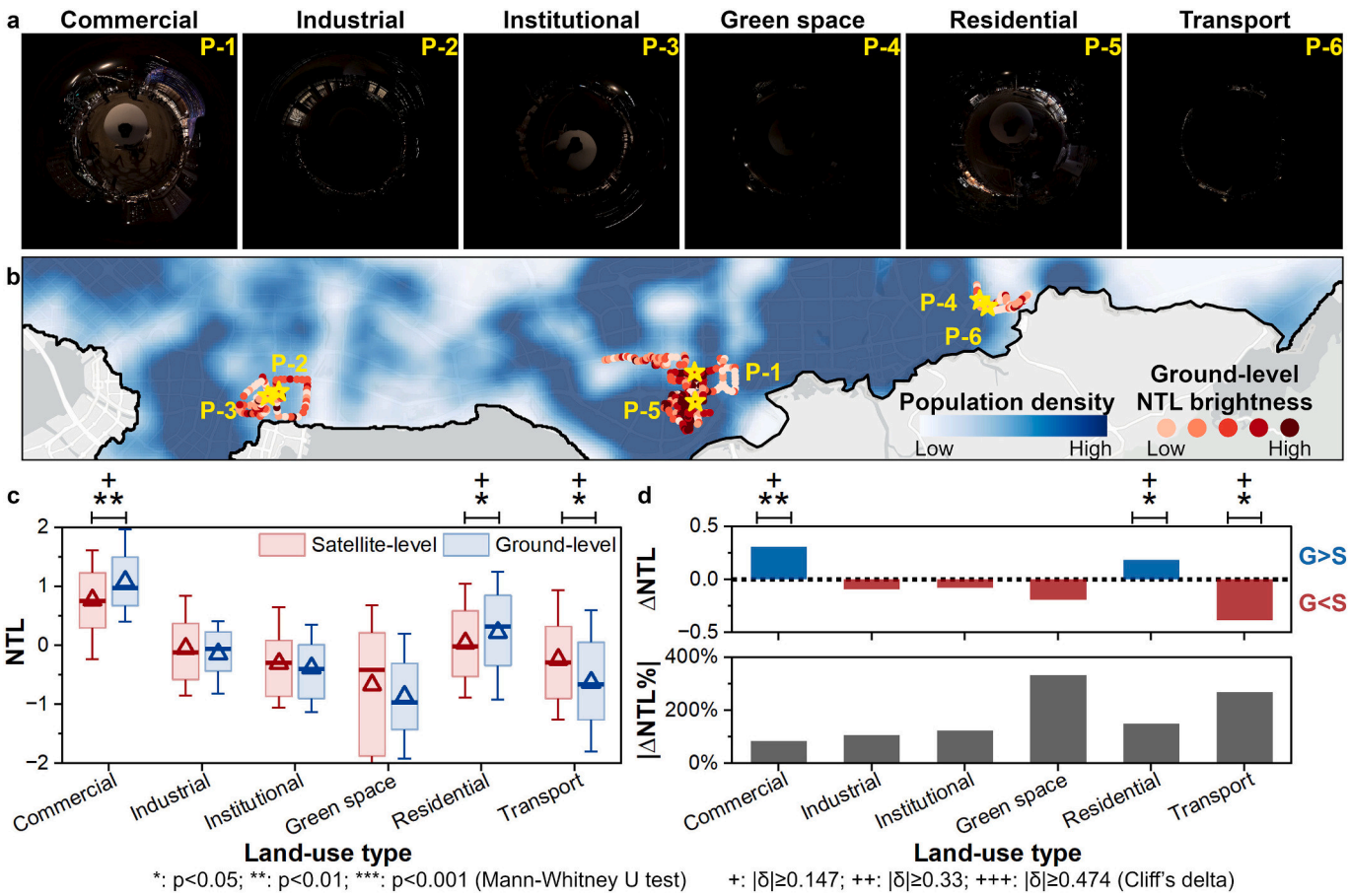

Fig. 11. Satellite-ground disagreement across land-use types in Shenzhen: (a) fisheye nighttime SVIs from the NightSVI-SZ dataset; (b) sampling sites; (c) z-scored satellite- and ground-level NTL brightness; (d) absolute disagreement (ΔNTL) and relative disagreement (|ΔNTL%|). (For interpretation of the references to colour in this figure legend, the reader is referred to the web version of this article.)

Table 1
OLS regression results.

Variable	(1)	(2)	(3)	(4)	(5)	(6)	(7)	(8)	(9)	(10)
	ΔNTL_{O_H12}						ΔNTL_{E_H12}		ΔNTL_{E_H10}	ΔNTL_{E_H8}
BVF		0.841***	0.615***	0.635***	0.805***	0.683***	2.654***	2.429***	2.097***	2.491***
		(0.156)	(0.136)	(0.159)	(0.157)	(0.165)	(0.010)	(0.009)	(0.043)	(0.426)
HW	0.005*		0.003	0.002	0.003	0.003	0.003***	0.002***	0.009***	−0.049***
	(0.002)		(0.002)	(0.002)	(0.002)	(0.002)	(0.001)	(0.000)	(0.001)	(0.013)
NDVI	−0.078	0.294*		0.336**	0.304*	0.459***	0.761***	0.321***	0.604***	0.022
	(0.115)	(0.129)		(0.130)	(0.129)	(0.138)	(0.009)	(0.009)	(0.036)	(0.160)
RG	−0.112***	−0.126***	−0.130***		−0.128***	−0.127***	0.000	−0.002***	−0.014***	0.011
	(0.022)	(0.022)	(0.022)		(0.022)	(0.023)	(0.001)	(0.001)	(0.003)	(0.019)
RB	0.009**	0.011**	0.011**		0.011**	0.009*	0.000**	0.000	−0.004***	−0.020***
	(0.003)	(0.003)	(0.003)		(0.003)	(0.003)	(0.000)	(0.000)	(0.000)	(0.003)
N	1148	1148	1148	1148	1148	1148	361,954	361,954	19,593	718
Land-use fixed effects	N	N	N	N	N	Y	N	Y	N	N
R^2	0.030	0.050	0.048	0.017	0.052	0.072	0.287	0.349	0.211	0.148

Note: ΔNTL_O: absolute disagreement derived from observed ground-level NTL brightness using the NightSVI-SG_{Fan} dataset; ΔNTL_E: absolute disagreement derived from RF-estimated ground-level NTL brightness. H12, H10, and H8 indicate the corresponding analytical resolutions. *: $p < 0.05$; **: $p < 0.01$; ***: $p < 0.001$. Columns (1)–(10) represent different model specifications and analytical resolutions.

storefront lighting at the base of residential buildings (Fig. 16). By contrast, transport areas predominantly exhibited the G<S pattern, potentially because ground-level sensors capture locally visible, discrete road lighting (e.g., individual street lamps), whereas satellite imagery captures NTL signals from more spatially continuous road surfaces, with SDGSAT-1 NTL imagery showing particular sensitivity to road illumination that has been widely exploited for road extraction and mapping (Wang et al., 2026a; Wu et al., 2024).

Building on these findings, this study advances existing knowledge in three aspects. First, previous studies have predominantly relied on spatially discrete, sample-based ground-level observations to compare satellite- and ground-level NTL measurements (Katz and Levin, 2016; Levin, 2023). For instance, Labrousse et al. (2025) focused on a major road interchange in Israel and revealed asymmetric patterns between satellite- and ground-level observations when quantifying the impact of LED retrofits. By extending such comparisons from discrete sites to a spatially continuous, citywide assessment, our study contributes to a wall-to-wall characterization of the spatial heterogeneity of satellite-

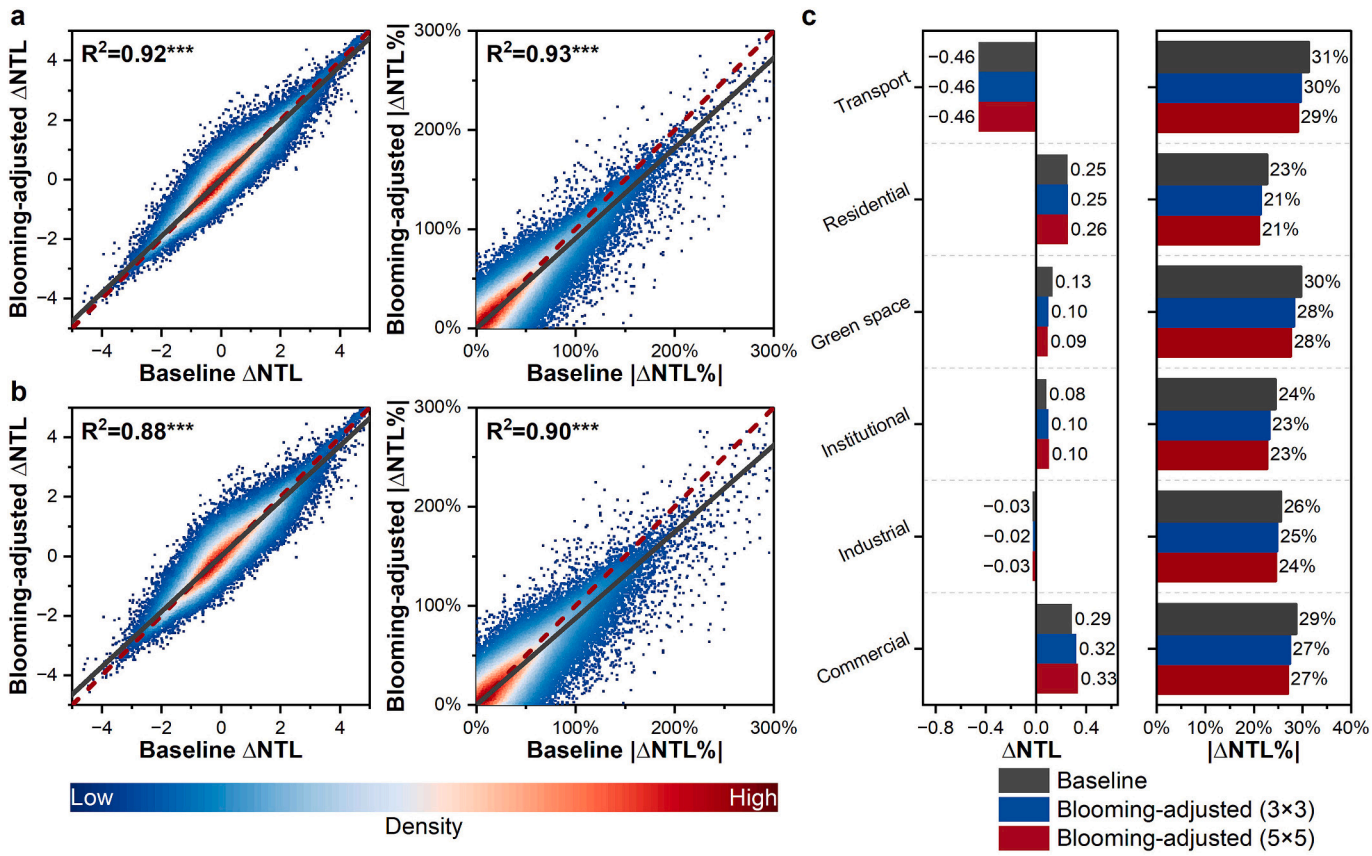

Fig. 12. Analysis of the blooming effect at the H12 resolution: (a) blooming-adjusted versus baseline estimates using a 3 × 3 moving window; (b) blooming-adjusted versus baseline estimates using a 5 × 5 moving window; (c) comparison of satellite-ground disagreement across land-use types. Corresponding results at the H8 and H10 resolutions are presented in Fig. S7. In (a–b), the red dashed lines indicate the 1:1 relationship, whereas the dark gray lines represent zero-intercept linear fits. *: $p < 0.05$; **: $p < 0.01$; ***: $p < 0.001$. (For interpretation of the references to colour in this figure legend, the reader is referred to the web version of this article.)

ground disagreement across Singapore. This transition reduces sensitivity to sparse sampling and, more importantly, brings diverse urban contexts into a unified analytical framework, enabling more systematic and comparable assessments of satellite-ground disagreement across the full spectrum of urban environments.

Second, we establish a scalable framework for estimating ground-level NTL brightness from panoramic nighttime SVIs. Existing studies have inferred ground-level lighting conditions by extracting deep features from daytime SVI (Fan and Biljecki, 2024) or using image generation algorithms (e.g., Pix2Pix, Stable Diffusion, and CycleGAN) (Liu et al., 2024; Wang et al., 2026b; Ye et al., 2025). Our approach complements these methods by being grounded in the physical mechanisms of NTL remote sensing and by propagating estimation uncertainty into satellite-ground disagreement, thereby allowing the robustness of the identified disagreement patterns to be explicitly quantified.

Third, moving beyond the characterization of spatially heterogeneous satellite-ground disagreement, this study delves further into its underlying contributing factors and implications for downstream NTL applications. Such mechanism-informed interpretation and impact assessments establish a more integrated analytical framework for satellite-ground disagreement, broadening the scope of previous studies and providing a stronger empirical basis for comparing different NTL observations in remote sensing.

5.2. Implications of satellite-ground disagreement for NTL observations and applications

Our systematic investigation brings to light pronounced local satellite-ground disagreement otherwise concealed by citywide averages. Importantly, such disagreement is context-dependent and bidirectional, with distinct G>S and G<S patterns across land-use types. These findings highlight observation approach as a fundamental dimension of variability in NTL remote sensing. Treating satellite- and ground-level NTL observations as interchangeable, or overlooking the spatial heterogeneity of the disagreement, can introduce substantial and spatially structured uncertainty into NTL-based studies. In an era of increasingly available multi-source NTL data, this underscores the need for a multi-level analytical framework that jointly interprets different NTL observations, enabling a more holistic representation of nighttime environment and more comprehensive urban nighttime auditing and modeling.

Beyond NTL observations, our findings also hold significant implications for NTL-based applications and policymaking. First, satellite-ground disagreement exhibited clear scale effects, manifested by the progressively increasing magnitude of disagreement toward finer analytical resolutions. This may be attributable to the influence of spatial aggregation: coarser resolutions tend to smooth localized extremes, whereas finer resolutions preserve greater heterogeneity. Such scale effects corroborate previous evidence from multi-resolution comparisons of NTL observations in remote sensing (Guk and Levin, 2020; Guo et al., 2023b). Importantly, these suggest that the more nuanced spatial representation enabled by high-resolution NTL data does not necessarily imply greater consistency across sensing approaches. As high-resolution NTL products (e.g., SDGSAT-1) are increasingly used in urban and environmental applications, greater attention should be paid to potentially amplified satellite-ground disagreement, which may affect assessments of NTL exposure experienced by humans and ecosystems.

Second, our analysis across land-use types reveals consistently

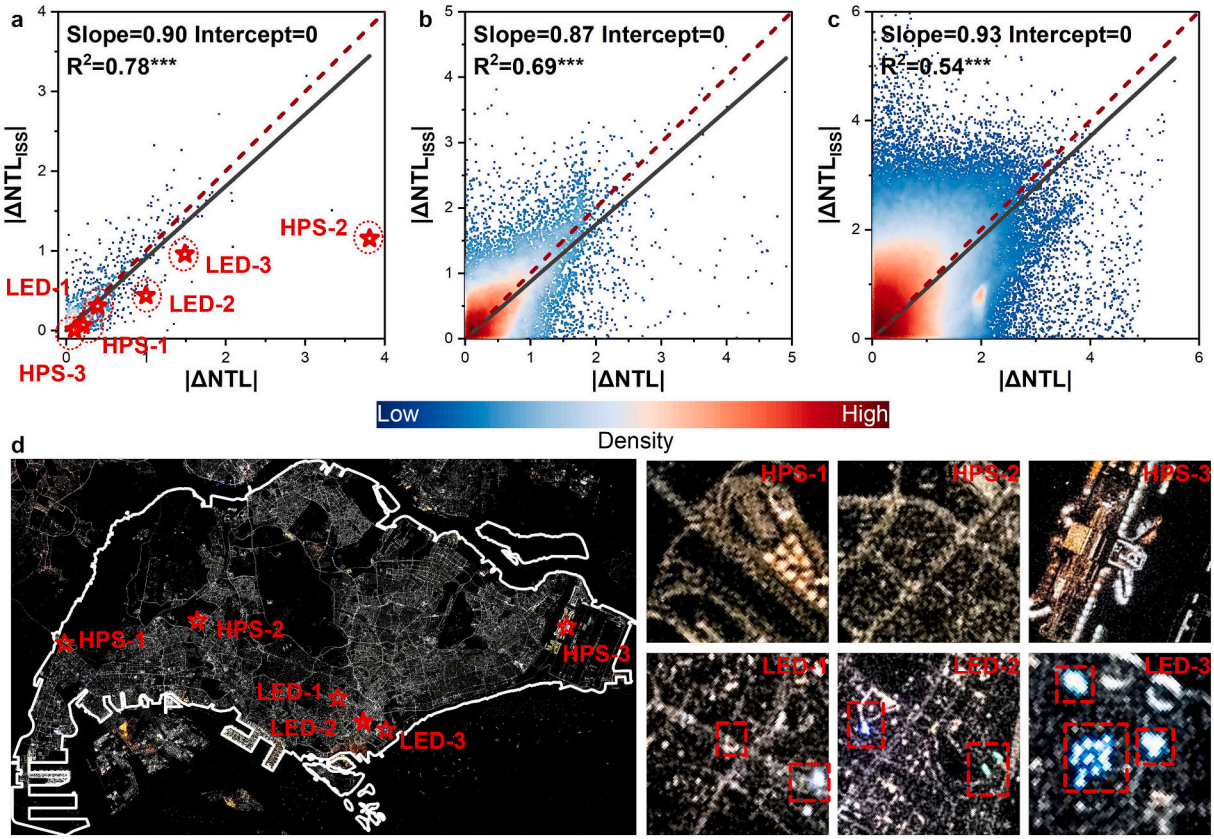

Fig. 13. Analysis of sensor spectral response: (a–c) $|\Delta NTL_{ISS}|$ versus $|\Delta NTL|$; (d) multispectral ISS NTL imagery. In (a–c), the red dashed lines indicate the 1:1 relationship, whereas the dark gray lines represent zero-intercept linear fits. *: $p < 0.05$; **: $p < 0.01$; ***: $p < 0.001$. (For interpretation of the references to colour in this figure legend, the reader is referred to the web version of this article.)

pronounced satellite-ground disagreement in commercial areas, raising particular concerns for NTL-based studies given the prominence of commercial areas as light pollution hotspots. Such disagreement suggests that satellite observations may not fully capture the complexity of lighting environments where reliable monitoring is most imperative, yielding source-dependent assessments of lighting conditions and intervention effectiveness. This issue is further complicated by the increasing use of satellite-level NTL data to evaluate lighting regulations and management, such as Tucson's municipal dimming program and lighting mitigation policies in Florida (Kyba et al., 2021; McDermott, 2023).

Finally, building morphology, particularly BVF, exhibited a substantially more stable association with satellite-ground disagreement. Compared with HW, which describes street-canyon geometry, BVF more directly represents visible building obstruction from a human-scale vantage point, highlighting the importance of three-dimensional urban morphology and viewing geometry in NTL remote sensing. Sensor spectral response also contributed to the observed disagreement, which matters for the design of future NTL-dedicated satellites, particularly the need for enhanced sensitivity to blue-light emissions (Weber et al., 2025). As LED retrofits continue to proliferate, the limited blue-light sensitivity of current satellite sensors (e.g., SDGSAT-1, VIIRS, and Luojia-1) may underrepresent LED-dominated lighting conditions, especially in countries undergoing extensive lighting transitions, such as the United States, Bulgaria, and Italy (de Miguel et al., 2019; Hung et al., 2021; Tsankov et al., 2025).

Overall, relying solely on satellite-level NTL data may not always be sufficient, particularly in areas with substantial satellite-ground disagreement. Our study provides an essential prerequisite for reliable multi-level NTL data integration, enabling end users to better interpret observed NTL brightness patterns and draw more appropriate conclusions for specific applications.

5.3. Limitations and future work

While this study employed nighttime SVIs to characterize ground-level NTL brightness, alternative instruments such as SQMs may generate different satellite-ground disagreement patterns because they capture distinct aspects of the nighttime environment. SQMs are often installed on building rooftops to measure sky brightness and lack spectral signatures, despite their high sensitivity under low-light conditions (Levin, 2025; Pun and So, 2012; Pun et al., 2014). Accordingly, the identified disagreement patterns in this study should be interpreted in relation to the specific ground-level observation approach adopted.

We acknowledge that nighttime SVIs and SDGSAT-1 imagery were not acquired in strict temporal synchrony, which may introduce temporal uncertainty into the analysis. To address this, SVI acquisition was consistently concentrated within peak nighttime hours (20:00–23:00 local time), when lighting conditions are relatively stable before widespread dimming (Li et al., 2020a). Additionally, recent evidence indicates that simultaneous ground-level measurements do not necessarily yield stronger agreement with satellite-level observations than measurements acquired on separate nights (Levin et al., 2026). We therefore expect the temporal uncertainty to be limited. Moreover, given the dense sampling interval (10 m) and availability of GSV images, a minor proportion of areas, such as airports and remote reservoirs, were

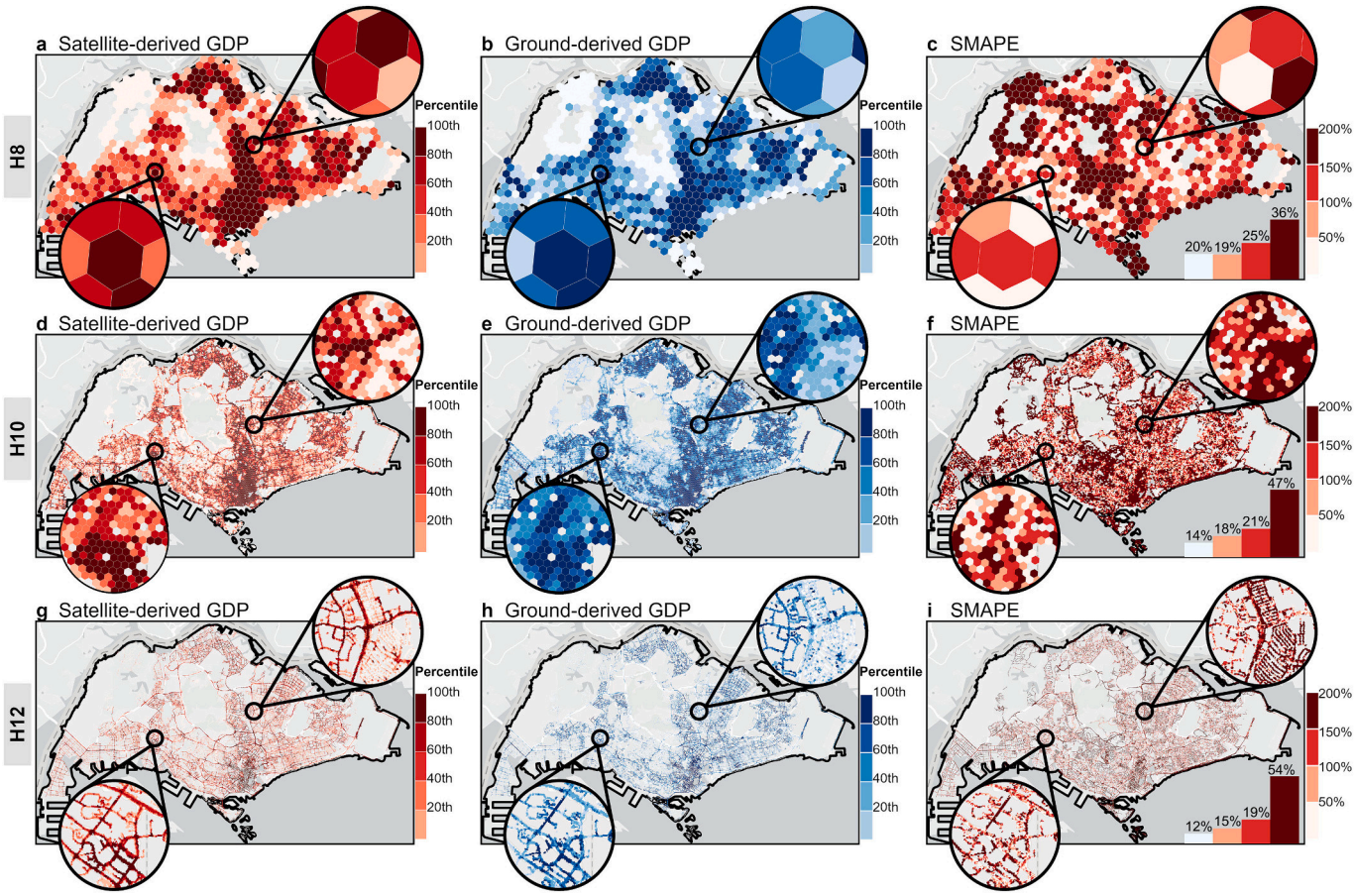

Fig. 14. GDP estimates: (a, d, g) satellite-derived GDP; (b, e, h) ground-derived GDP; (c, f, i) SMAPE values. (For interpretation of the references to colour in this figure legend, the reader is referred to the web version of this article.)

excluded from our analysis. We believe this has trivial impact on our findings, as the retained areas cover a sufficiently broad range of lighting conditions and urban contexts across Singapore.

Ultimately, although Singapore and Shenzhen differ in their urban characteristics, both are highly urbanized cities. The extent to which the identified disagreement patterns transfer to rural, low-light, or less-developed areas therefore requires further scrutiny. Although the proposed framework is inherently transferable, its broader application is currently constrained by the limited availability of nighttime SVI, a common challenge in SVI-based studies (Dai et al., 2026; Wang et al., 2026b). Currently available SVI is primarily acquired during the daytime, with nighttime SVI comprising only about 3.1% (Hou et al., 2024). Moreover, inconsistent camera settings (e.g., ISO and exposure) further hinder the utility of existing nighttime SVI. Acknowledging this limitation, this study prioritized manually collected nighttime SVI in Singapore and Shenzhen under fixed camera settings, and underscored the need for coordinated efforts to develop a global standardized NTL observation network.

6. Conclusion

As NTL observations become increasingly available for monitoring urban development, differences in observation approaches can produce markedly different representations of nighttime lighting patterns. Through a spatially explicit, wall-to-wall investigation, this study demonstrates that satellite-ground disagreement is not a spatially uniform measurement offset, but rather exhibits pronounced heterogeneity across the city and land-use types, supported by uncertainty quantification and sensitivity analyses. Commercial and residential areas exhibited consistent G>S disagreement patterns, while transport areas showed the opposite G<S pattern, with relative disagreement of 23%–31% across these land-use types. Building morphology, vegetation canopy cover, and sensor spectral response significantly contributed to satellite-ground disagreement. The use of satellite- and ground-level NTL data produced substantial differences in downstream applications, with relative differences of at least 115% and 83% in GDP estimation and NTL exposure inequality assessment, respectively.

This study highlights the importance of integrating complementary NTL observations to support a more holistic and nuanced characterization of nighttime lighting environment, and strengthens the foundation for more reliable NTL-based applications and sustainable urbanization (e.g., energy efficiency and urban lighting management). Future studies could benefit from broader acquisition of nighttime SVIs under standardized measurement protocols and with comprehensive imaging metadata, incorporation of human-scale perception data to better interpret the nighttime environment experienced by residents, and

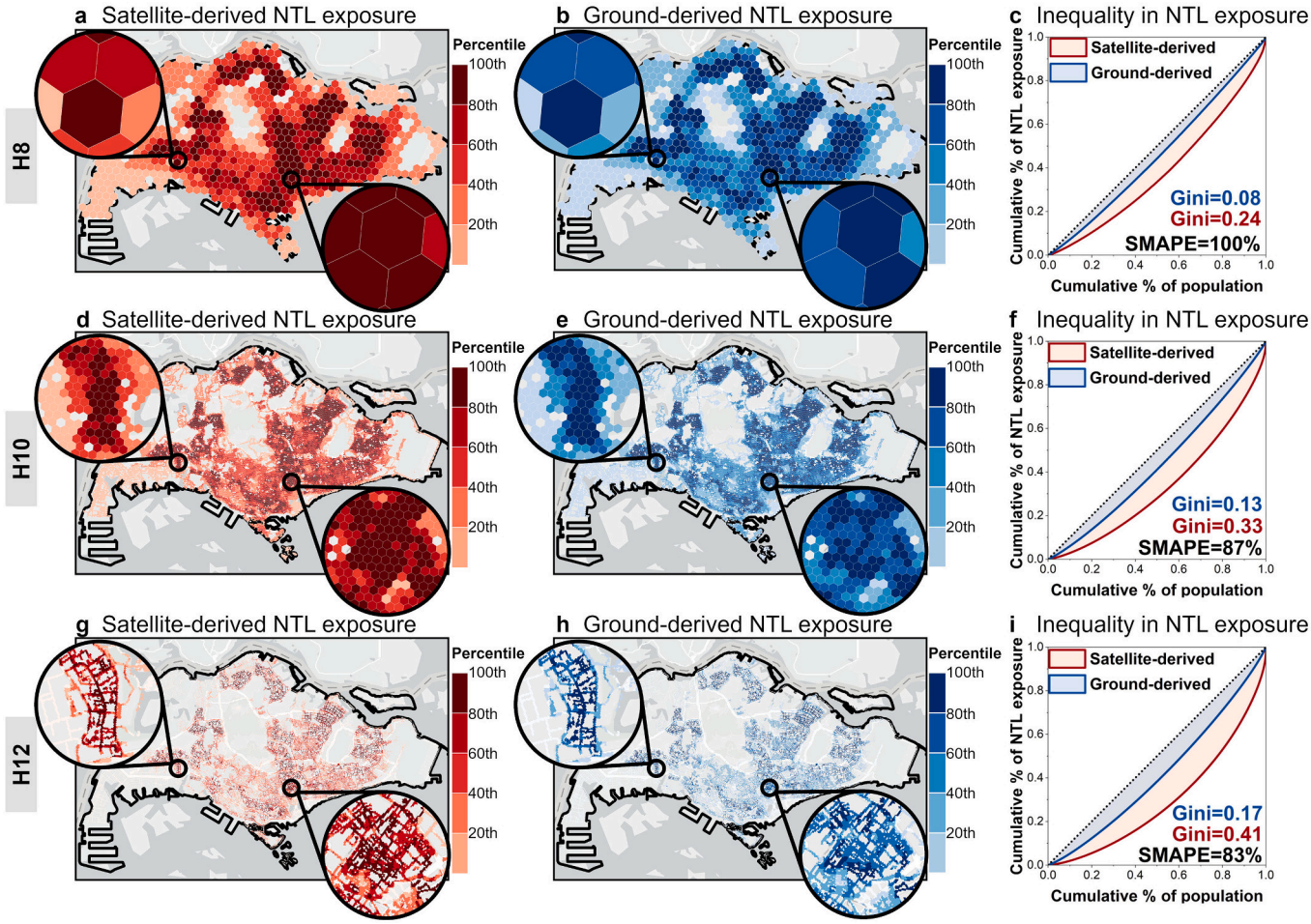

Fig. 15. Total NTL exposure: (a, d, g) satellite-derived NTL exposure; (b, e, h) ground-derived NTL exposure; (c, f, i) Lorenz curves with Gini coefficients. Percentile-based classes were used to facilitate visualization across the wide range of NTL exposure values, with the same scheme applied to Fig. 14 for consistency. (For interpretation of the references to colour in this figure legend, the reader is referred to the web version of this article.)

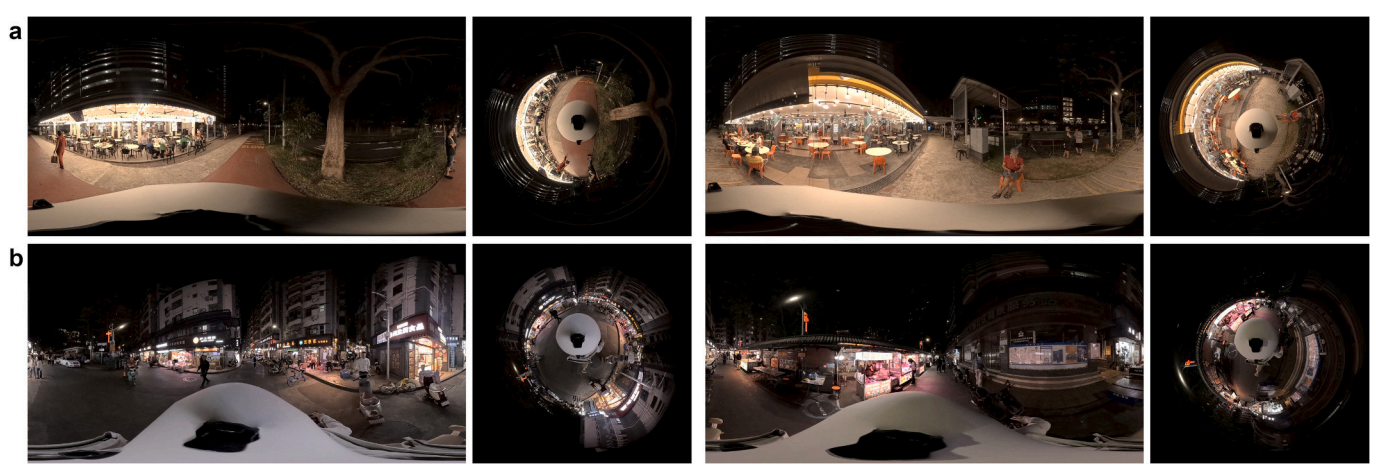

Fig. 16. Examples of nighttime SVIs: (a) hawker centers in Singapore; (b) ground-floor shops in Shenzhen. (For interpretation of the references to colour in this figure legend, the reader is referred to the web version of this article.)

development of integration frameworks for downstream applications.

CRediT authorship contribution statement

Yu Gong: Conceptualization, Methodology, Formal analysis, Visualization, Writing – original draft, Writing – review & editing. **Qiming Zheng:** Conceptualization, Methodology, Writing – original draft, Writing – review & editing, Funding acquisition, Supervision. **Filip Biljecki:** Conceptualization, Writing – review & editing. **Waishan Qiu:** Conceptualization, Writing – review & editing. **Zicheng Fan:** Conceptualization, Writing – review & editing, Data curation. **Zihao Zheng:** Writing – review & editing. **Lin Yan:** Resources, Writing – review &

editing. **Chun Shing Jason Pun:** Writing – review & editing. **Sylvia Y. He:** Writing – review & editing, Supervision.

Declaration of competing interest

The authors declare that they have no known competing financial interests or personal relationships that could have appeared to influence the work reported in this paper.

Acknowledgements

Qiming Zheng is supported by the Chinese University of Hong Kong (4937239, 4750495, and 4052360) and the National Natural Science Foundation of China (42501403). We sincerely thank the International Research Center of Big Data for Sustainable Development Goals (CBAS) for sharing the SDGSAT-1 glimmer data.

Appendix A. Supplementary data

Supplementary data to this article can be found online at https://doi.org/10.1016/j.rse.2026.115724.

Data availability

The NightSVI-SG_{Fan} dataset is available at https://github.com/zichengfan/Nighttime-SVI/tree/main. The NightSVI-SG_{Yu} and NightSVI-SZ datasets are available via email request to the corresponding author.

References

Amaral, S., Câmara, G., Monteiro, A.M.V., Quintanilha, J.A., Elvidge, C.D., 2005. Estimating population and energy consumption in Brazilian Amazonia using DMSP night-time satellite data. Comput. Environ. Urban. Syst. 29 (2), 179–195.
Aubé, M., Marseille, C., Farkouh, A., Dufour, A., Simoneau, A., Zamorano, J., Roby, J., Tapia, C., 2020. Mapping the melatonin suppression, star light and induced photosynthesis indices with the LANcube. Remote Sensing 12 (23), 3954.
Biljecki, F., Ito, K., 2021. Street view imagery in urban analytics and GIS: a review. Landsc. Urban Plan. 215, 104217.
Bousquin, J., 2021. Discrete Global Grid Systems as scalable geospatial frameworks for characterizing coastal environments. Environ. Model. Softw. 146, 105210.
CBAS, 2022. SDGSAT-1 Data Users Handbook (Draft). http://60.245.209.56/preview/20221125/c84c0b5d89984cd384ffa05dbb163d14.pdf.
Chen, Z., Cheng, L., Chen, Y., Wu, J., Tu, Y., 2026. Identifying composite spatial patterns of China's shrinking cities from nighttime light remote sensing. GISci. Remote Sens. 63 (1), 2605710.
Chen, Z., Li, P., Jin, Y., Jin, Y., Chen, J., Li, W., Song, X., Shibasaki, R., Chen, M., Yan, D., 2022. Using mobile phone big data to identify inequity of artificial light at night exposure: a case study in Tokyo. Cities 128, 103803.
Cliff, N., 1993. Dominance statistics: ordinal analyses to answer ordinal questions. Psychol. Bull. 114 (3), 494.
Dai, J., Wang, Y., Qiu, W., Ma, J., Chen, D., 2026. The urban greening paradox: measuring day-night perceived safety divergences from paired street view images using generative AI. Urban For. Urban Green. 118, 129350.
de Miguel, A.S., Kyba, C.C., Aubé, M., Zamorano, J., Cardiel, N., Tapia, C., Bennie, J., Gaston, K.J., 2019. Colour remote sensing of the impact of artificial light at night (I): the potential of the International Space Station and other DSLR-based platforms. Remote Sens. Environ. 224, 92–103.
de Miguel, A.S., Zamorano, J., Aubé, M., Bennie, J., Gallego, J., Ocaña, F., Pettit, D.R., Stefanov, W.L., Gaston, K.J., 2021. Colour remote sensing of the impact of artificial light at night (part II): calibration of DSLR-based images from the International Space Station. Remote Sens. Environ. 264, 112611.
Elvidge, C.D., Keith, D.M., Tuttle, B.T., Baugh, K.E., 2010. Spectral identification of lighting type and character. Sensors 10 (4), 3961–3988.
Falchi, F., Cinzano, P., Duriscoe, D., Kyba, C.C., Elvidge, C.D., Baugh, K., Portnov, B.A., Rybnikova, N.A., Furgoni, R., 2016. The new world atlas of artificial night sky brightness. Sci. Adv. 2 (6), e1600377.
Fan, Z., Biljecki, F., 2024. Nighttime street view imagery: a new perspective for sensing urban lighting landscape. Sustain. Cities Soc. 116, 105862.
Fang, G., Gao, Z., Tian, L., Fu, M., 2022. What drives urban carbon emission efficiency?–spatial analysis based on nighttime light data. Appl. Energy 312, 118772.
Gao, B., Huang, Q., He, C., Sun, Z., Zhang, D., 2016. How does sprawl differ across cities in China? A multi-scale investigation using nighttime light and census data. Landsc. Urban Plan. 148, 89–98.
Gong, Y., Li, X., Li, D., Zhang, X., 2025. Urban recovery patterns after the 2023 Turkey-Syria earthquake revealed by SDGSAT-1 nighttime light data. Remote Sens. Environ. 328, 114888.
Guk, E., Levin, N., 2020. Analyzing spatial variability in night-time lights using a high spatial resolution color Jilin-1 image–Jerusalem as a case study. ISPRS J. Photogram. Remote Sensing 163, 121–136.
Guo, B., Hu, D., Zheng, Q., 2023b. Potentiality of SDGSAT-1 glimmer imagery to investigate the spatial variability in nighttime lights. Int. J. Appl. Earth Observ. Geoinform. 119, 103313.
Guo, H., Dou, C., Chen, H., Liu, J., Fu, B., Li, X., Zou, Z., Liang, D., 2023a. SDGSAT-1: the world's first scientific satellite for sustainable development goals. Sci. Bull. 68 (1), 34–38.
He, M., Xu, Q., Wang, W., Shao, Z., Li, X., 2023. Multiscale estimation of electrification rate using night-time light imagery. IEEE J. Select. Top. Appl. Earth Observ. Remote Sens. 16, 8960–8968.
Helbich, M., Poppe, R., Oberski, D., van Emmichoven, M.Z., Schram, R., 2021. Can't see the wood for the trees? An assessment of street view-and satellite-derived greenness measures in relation to mental health. Landsc. Urban Plan. 214, 104181.
Ho, C., Lin, H., 2015. Analysis of and control policies for light pollution from advertising signs in Taiwan. Light. Res. Technol. 47 (8), 931–944.
Hou, Y., Quintana, M., Khomiakov, M., Yap, W., Ouyang, J., Ito, K., Wang, Z., Zhao, T., Biljecki, F., 2024. Global streetscapes—a comprehensive dataset of 10 million street-level images across 688 cities for urban science and analytics. ISPRS J. Photogramm. Remote Sens. 215, 216–238.
Huang, H., Wu, B., Wang, Y., Yu, B., Huang, H., Zhang, W., 2025. Towards building floor-level nighttime light exposure assessment using SDGSAT-1 GLI data. ISPRS J. Photogram. Remote Sens. 223, 375–397.
Hung, L.-W., Anderson, S.J., Pipkin, A., Fristrup, K., 2021. Changes in night sky brightness after a countywide LED retrofit. J. Environ. Manage. 292, 112776.
Jia, M., Zeng, H., Chen, Z., Wang, Z., Ren, C., Mao, D., Zhao, C., Zhang, R., Wang, Y., 2024. Nighttime light in China's coastal zone: the type classification approach using SDGSAT-1 Glimmer Imager. Remote Sens. Environ. 305, 114104.
Jiang, Y., Tang, Y., Jing, L., Galdies, C., Li, H., Yan, L., Ding, H., Xie, Q., Dou, C., 2024. Urban nighttime aerosol optical depth retrieval methods from SDGSAT-1 glimmer data. Int. J. Digit. Earth 17 (1), 2411822.
Kamath, H.G., Singh, M., Malviya, N., Martilli, A., He, L., Aliaga, D., He, C., Chen, F., Magruder, L.A., Yang, Z.-L., 2024. Global building heights for urban studies (UT-GLOBUS) for city-and street-scale urban simulations: development and first applications. Sci. Data 11 (1), 886.
Kang, Y., Zhang, F., Gao, S., Lin, H., Liu, Y., 2020. A review of urban physical environment sensing using street view imagery in public health studies. Ann. GIS 26 (3), 261–275.
Katz, Y., Levin, N., 2016. Quantifying urban light pollution—a comparison between field measurements and EROS-B imagery. Remote Sens. Environ. 177, 65–77.
Kocifaj, M., 2018. Towards a comprehensive city emission function (CCEF). J. Quant. Spectrosc. Radiat. Transf. 205, 253–266.
Kocifaj, M., Wallner, S., Barentine, J.C., 2023. Measuring and monitoring light pollution: current approaches and challenges. Science 380 (6650), 1121–1124.
Kyba, C., Ruhtz, T., Fischer, J., Hölker, F., 2012. Red is the new black: how the colour of urban skyglow varies with cloud cover. Mon. Not. R. Astron. Soc. 425 (1), 701–708.
Kyba, C.C., Ruby, A., Kuechly, H., Kinzey, B., Miller, N., Sanders, J., Barentine, J., Kleinodt, R., Espey, B., 2021. Direct measurement of the contribution of street lighting to satellite observations of nighttime light emissions from urban areas. Light. Res. Technol. 53 (3), 189–211.
Labrousse, C., Haspel, C., Levin, N., 2025. Quantifying the impact of the transition to LED lighting on night sky brightness and colour using ground-based measurements and satellite imagery. J. Quant. Spectrosc. Radiat. Transf. 340, 109450.
Levin, N., 2023. Quantifying the variability of ground light sources and their relationships with spaceborne observations of night lights using multidirectional and multispectral measurements. Sensors 23 (19), 8237.
Levin, N., 2025. Challenges in remote sensing of night lights–a research agenda for the next decade. Remote Sens. Environ. 328, 114869.
Levin, N., Kyba, C.C., Zhang, Q., de Miguel, A.S., Román, M.O., Li, X., Portnov, B.A., Molthan, A.L., Jechow, A., Miller, S.D., 2020. Remote sensing of night lights: a review and an outlook for the future. Remote Sens. Environ. 237, 111443.
Levin, N., Lin, Y., Li, X.-M., Tang, Y., Wang, N., 2026. Ground referencing night time light imagery—how critical is it to conduct the measurements at the same time the image is acquired? Remote Sensing 18 (13), 2071.
Li, J., Li, X., Li, D., 2025. Impact of vegetation phenology on anisotropy of artificial light at night-evidence from multi-angle satellite observations. Remote Sens. Environ. 317, 114525.
Li, J., Xu, Y., Cui, W., Ji, M., Su, B., Wu, Y., Wang, J., 2020b. Investigation of nighttime light pollution in Nanjing, China by mapping illuminance from field observations and Luojia 1-01 imagery. Sustainability 12 (2), 681.
Li, T., Wang, Z., Kyba, C., Román, M.O., Seto, K.C., Yang, Y., Qiu, S., Kuester, T., Fragkias, M., Chen, X., 2026. Satellite imagery reveals increasing volatility in human night-time activity. Nature 652 (8109), 379–386.
Li, X., Levin, N., Xie, J., Li, D., 2020a. Monitoring hourly night-time light by an unmanned aerial vehicle and its implications to satellite remote sensing. Remote Sens. Environ. 247, 111942.
Li, X., Shang, X., Zhang, Q., Li, D., Chen, F., Jia, M., Wang, Y., 2022. Using radiant intensity to characterize the anisotropy of satellite-derived city light at night. Remote Sens. Environ. 271, 112920.
Lin, M., Lucas Jr., H.C., Shmueli, G., 2013. Research commentary—too big to fail: large samples and the p-value problem. Inf. Syst. Res. 24 (4), 906–917.
Liu, Y., Heuvelink, G.B., Bai, Z., He, P., 2023. Uncertainty quantification of nitrogen use efficiency prediction in China using Monte Carlo simulation and quantile regression forests. Comput. Electron. Agric. 204, 107533.

Liu, Z., Li, T., Ren, T., Chen, D., Li, W., Qiu, W., 2024. Day-to-night street view image generation for 24-hour urban scene auditing using generative AI. J. Imaging 10 (5), 112.
Luginbuhl, C.B., Duriscoe, D.M., Moore, C.W., Richman, A., Lockwood, G.W., Davis, D.R., 2009. From the ground up II: sky glow and near-ground artificial light propagation in Flagstaff, Arizona. Publ. Astron. Soc. Pac. 121 (876), 204.
McDermott, A., 2023. Light pollution is fixable. Can researchers and policymakers work together to dim the lights? Proc. Natl. Acad. Sci. 120 (27), e2309539120.
Meinshausen, N., Ridgeway, G., 2006. Quantile regression forests. J. Mach. Learn. Res. 7 (6).
Muñoz-Gil, G., Dauphin, A., Beduini, F.A., Sánchez de Miguel, A., 2022. Citizen science to assess light pollution with mobile phones. Remote Sens. 14 (19), 4976.
Ngarambe, J., Kim, G., 2018. Sustainable lighting policies: the contribution of advertisement and decorative lighting to local light pollution in Seoul, South Korea. Sustainability 10 (4), 1007.
Pan, W., Du, J., 2021. Impacts of urban morphological characteristics on nocturnal outdoor lighting environment in cities: an empirical investigation in Shenzhen. Build. Environ. 192, 107587.
Pun, C.S.J., So, C.W., 2012. Night-sky brightness monitoring in Hong Kong: a city-wide light pollution assessment. Environ. Monit. Assess. 184 (4), 2537–2557.
Pun, C.S.J., So, C.W., Leung, W.Y., Wong, C.F., 2014. Contributions of artificial lighting sources on light pollution in Hong Kong measured through a night sky brightness monitoring network. J. Quant. Spectrosc. Radiat. Transf. 139, 90–108.
Romano, J., Kromrey, J.D., Coraggio, J., Skowronek, J., 2006. Appropriate statistics for ordinal level data: should we really be using t-test and Cohen's d for evaluating group differences on the NSSE and other surveys. In: Annual Meeting of the Florida Association of Institutional Research.
Shi, K., Chen, Y., Yu, B., Xu, T., Yang, C., Li, L., Huang, C., Chen, Z., Liu, R., Wu, J., 2016. Detecting spatiotemporal dynamics of global electric power consumption using DMSP-OLS nighttime stable light data. Appl. Energy 184, 450–463.
Shi, K., Ma, J., Chen, Z., Cui, Y., Yu, B., 2023. Nighttime light remote sensing in characterizing urban spatial structure. Innov. Geosci. 1 (3).
Shi, X., Kocifaj, M., Li, X., Li, D., Li, J., 2025. Impact of atmospheric effect and observation geometry on the directional distribution of blooming effect in VIIRS night-time light images. Remote Sens. Environ. 331, 115017.
Tan, M., Li, X., Li, S., Xin, L., Wang, X., Li, Q., Li, W., Li, Y., Xiang, W., 2018. Modeling population density based on nighttime light images and land use data in China. Appl. Geogr. 90, 239–247.
Tan, X., Zhu, X., Chen, J., Chen, R., 2022. Modeling the direction and magnitude of angular effects in nighttime light remote sensing. Remote Sens. Environ. 269, 112834.
Tsankov, P., Yovchev, M., Ibrishimov, H., 2025. Energy-efficient light-emitting diode retrofit and advanced control in municipal street lighting: a case study from Bulgaria. Asian J. Water Environ. Pollut. 22 (6), 180–197.
Wallner, S., Kocifaj, M., 2019. Impacts of surface albedo variations on the night sky brightness–a numerical and experimental analysis. J. Quant. Spectrosc. Radiat. Transf. 239, 106648.
Wang, C., Xu, W., Chen, Z., Liu, S., Li, W., Zhang, L., Gao, S., Huang, Y., Wu, J., Yu, B., 2025. STARS: a novel gap-filling method for SDGSAT-1 nighttime light imagery using spatiotemporal and spectral synergy. Remote Sens. Environ. 322, 114720.
Wang, N., Hu, Y., Li, X.-M., Lan, Y., Kang, C., Yan, L., Dou, C., Miao, C., 2024. Enhancing SDGSAT-1 night light images using a panchromatic guidance denoising algorithm. Int. J. Appl. Earth Obs. Geoinf. 128, 103748.
Wang, Y., Li, J., Huang, H., Zhang, Z., Huang, H., Zhang, W., Wu, B., 2026a. A local CSF-based method for extracting illuminated urban roads from SDGSAT-1 nighttime light data. Remote Sens. Environ. 340, 115434.
Wang, Y., Xiang, Y., Ma, H., Lu, Y., Chen, Z., Qiu, W., 2026b. Nightlight-nightlife interplay: the threshold effect of ambient lighting on perceived safety and physical activity at night. Int. J. Appl. Earth Observ. Geoinform. 147, 105146.
Wang, Z., Román, M.O., Kalb, V.L., Miller, S.D., Zhang, J., Shrestha, R.M., 2021. Quantifying uncertainties in nighttime light retrievals from Suomi-NPP and NOAA-20 VIIRS Day/Night Band data. Remote Sens. Environ. 263, 112557.
Weber, D., Bolliger, J., Ecker, K., Fischer, C., Ginzler, C., Gossner, M.M., Huber, L., Obrist, M.K., Zellweger, F., Levin, N., 2025. Night lights from space: potential of SDGSAT-1 for ecological applications. Remote Sens. Ecol. Conserv. 11 (5), 495–509.
Wei, M., Zhao, Y., Xu, J., Du, H., Li, X., Mao, F., 2025. Phenology-explicit remote sensing estimation of V25cmax spatiotemporal dynamics and uncertainty in Moso bamboo forests. Ecol. Indic. 181, 114469.
Wu, B., Wang, Y., Huang, H., Liu, S., Yu, B., 2024. Potential of SDGSAT-1 nighttime light data in extracting urban main roads. Remote Sens. Environ. 315, 114448.
Wu, J., Li, X., Li, D., 2025. Investigating the anisotropy of nighttime light using an unmanned aerial vehicle combined with scaled experiments. Remote Sens. Environ. 329, 114960.
Yan, L., Hu, Y., Dou, C., Li, X.-M., 2024. Radiometric calibration of SDGSAT-1 nighttime light payload. IEEE Trans. Geosci. Remote Sens. 62, 1–15.
Yang, S., Yang, X., Gao, X., Zhang, J., 2022. Spatial and temporal distribution characteristics of carbon emissions and their drivers in shrinking cities in China: empirical evidence based on the NPP/VIIRS nighttime lighting index. J. Environ. Manage. 322, 116082.
Ye, X., Wang, Y., Dai, J., Qiu, W., 2025. Generated nighttime street view image to inform perceived safety divergence between day and night in high density cities: a case study in Hong Kong. J. Urban Manage. 14 (2), 379–401.
Yeh, A.G., Yuen, B., 2010. Tall building living in high density cities: A comparison of Hong Kong and Singapore. In: High-Rise Living in Asian Cities. Springer, pp. 9–23.
Yin, Z., Li, X., Tong, F., Li, Z., Jendryke, M., 2020. Mapping urban expansion using night-time light images from Luojia1-01 and international Space Station. Int. J. Remote Sens. 41 (7), 2603–2623.
Zheng, Q., Weng, Q., Wang, K., 2020. Correcting the Pixel Blooming Effect (PiBE) of DMSP-OLS nighttime light imagery. Remote Sens. Environ. 240, 111707.